Behavioral/Cognitive

Decreasing Alertness Modulates Perceptual Decision-Making

Sridhar R. Jagannathan,[1] Corinne A. Bareham,[1,2,3,4] and Tristan A. Bekinschtein[1]

[1]Department of Psychology, University of Cambridge, Cambridge, CB2 3EB, United Kingdom, [2]Department of Clinical Neurosciences, University of Cambridge, Cambridge, CB2 0QQ, United Kingdom, [3]School of Psychology, Massey University, Palmerston North, 4474, New Zealand, and [4]School of Psychology, Victoria University of Wellington, Wellington, 6140, New Zealand

The ability to make decisions based on external information, prior knowledge, and evidence is a crucial aspect of cognition and may determine the success and survival of an organism. Despite extensive work on decision-making mechanisms/models, understanding the effects of alertness on neural and cognitive processes remain limited. Here we use EEG and behavioral modeling to characterize cognitive and neural dynamics of perceptual decision-making in awake/low alertness periods in humans (14 male, 18 female) and characterize the compensatory mechanisms as alertness decreases. Well-rested human participants, changing between full-wakefulness and low alertness, performed an auditory tone-localization task, and its behavioral dynamics were quantified with psychophysics, signal detection theory, and drift-diffusion modeling, revealing slower reaction times, inattention to the left side of space, and a lower rate of evidence accumulation in periods of low alertness. Unconstrained multivariate pattern analysis (decoding) showed a ~280 ms delayed onset driven by low alertness of the neural signatures differentiating between left and right decision, with a spatial reconfiguration from centroparietal to lateral frontal regions 150-360 ms. To understand the neural compensatory mechanisms with decreasing alertness, we connected the evidence-accumulation behavioral parameter to the neural activity, showing in the early periods (125-325 ms) a shift in the associated patterns from right parietal regions in awake, to right frontoparietal during low alertness. This change in the neurobehavioral dynamics for central accumulation-related cognitive processes defines a clear reconfiguration of the brain networks' regions and dynamics needed for the implementation of decision-making, revealing mechanisms of resilience of cognition when challenged by decreased alertness.

Key words: **alertness; arousal; attention; decision-making; evidence accumulation; reconfiguration**

Significance Statement

Most living organisms make multiple daily decisions, and these require a degree of evidence from both the environment and the internal milieu. Such decisions are usually studied under sequential sampling models and involve making a behavioral choice based on sensory encoding, central accumulation, and motor implementation processes. Since there is little research on how decreasing alertness affects such cognitive processes, this study has looked at the cognitive and neural dynamics of perceptual decision-making in people while fully awake and in drowsy periods. Using computational modeling of behavior and neural dynamics on human participants performing an auditory tone-localization task, we reveal how low alertness modulates evidence accumulation-related processes and its corresponding compensatory neural signatures.

Introduction

The question of how decisions are made has shaped the world's systems of government, justice, and social order (Buchanan and O'Connell, 2006). Studies on how the brain implements simple decisions have revealed several neurocognitive processes at the perceptual, central integration, and motor implementation levels (Sigman and Dehaene, 2005; O'Connell et al., 2018). However, the modulatory effects of the internal milieu, homeostasis, alertness, and circadian influences on such processes have received less attention (Knowles, 1993; Hull et al., 2003). Specifically, the effect of low alertness has only been tackled by sleep deprivation and brain injury studies but hardly by normal variations of wakefulness (Goupil and Bekinschtein, 2012).

Perceptual decision-making in cognitive sciences has been successfully studied (Link and Heath, 1975; Gold and Shadlen, 2007) under sequential sampling models (SSMs), and consists of

Received Jan. 25, 2021; revised Sep. 30, 2021; accepted Nov. 3, 2021.

Author contributions: S.R.J. and T.A.B. designed research; S.R.J., C.A.B., and T.A.B. performed research; S.R.J., C.A.B., and T.A.B. contributed unpublished reagents/analytic tools; S.R.J. analyzed data; S.R.J. wrote the first draft of the paper; S.R.J., C.A.B., and T.A.B. edited the paper; S.R.J. wrote the paper.

This work was supported by the Gates Cambridge Scholarship to S.R.J.; Wellcome Trust Biomedical Research Fellowship WT093811MA to T.A.B.; and small departmental funding to S.R.J. and T.A.B. We thank Annamaria Laudini and Dritan Nikolla for assistance with data collection; Andrés Canales-Johnson, Will Harrison, Valdas Noreika, and other members of the Consciousness and Cognition Lab in Cambridge for valuable comments and support; and Lavazza for continuous support with delicious and stimulating coffee.

S. R. Jagannathan's present address: Institute of Neurophysiology, Charité Universitätsmedizin Berlin, Berlin 10117, Germany.

The authors declare no competing financial interests.

Correspondence should be addressed to Sridhar R. Jagannathan at srj34@cam.ac.uk or Tristan A. Bekinschtein at tb419@cam.ac.uk.

https://doi.org/10.1523/JNEUROSCI.0182-21.2021

the following: (1) perceptual stage, a sensory system that transforms physical stimulus intensities to deliver decision-information; (2) central integration stage, a decision system that integrates and accumulates such decision-information variables and makes an optimal choice based on relative evidence; and (3) motor stage, a motor system that implements the appropriate motor plan/action. According to SSMs, accurate perceptual decisions separate the noise from the signal by repeatedly sampling and integrating evidence until there is enough in favor of one of the decision choices. The preferred concept to understand and develop a hypothesis is called the decision variable, and it is an accumulation of priors, evidence, internal milieu, and value into a quantity that is interpreted by the decision rule to produce a choice (Gold and Shadlen, 2007). This study aims to investigate how alertness modulates such decision mechanisms in spatial auditory perception.

To understand how alertness modulates perceptual decision-making, we need to first define the specific aspect of wakefulness to be used as the experimental manipulation (Bekinschtein et al., 2009b). Changes in alertness can be classified into "tonic" that span multiple trials/time periods, and "phasic" moment-to-moment changes produced in response to an ongoing task. A few recent studies have shown that alertness, measured by brainstem systems indirect markers (pupil response), modulates individual decision-making in moment-to-moment fluctuations (phasic) (McGinley et al., 2015; de Gee et al., 2017). Further to this, van Kempen et al. (2019) showed that lower tonic and higher phasic alertness via pupil measurements predicted shorter reaction times and was associated with a centroparietal positivity in EEG space. However, these studies have used pupil responses, which in neural terms is an indirect marker for alertness, and can also be influenced by stimulus features, such as visual contrast and several other parameters (Wang et al., 2018).

Studies in stroke patients have also revealed the effect of alertness on cognitive processes, such as spatial attention (Robertson et al., 1998). In particular, lesions on one side of the brain create a difficulty in localizing and paying attention to information on the side opposite to the lesion, a condition referred to as unilateral spatial neglect and usually more persistent after a stroke in the right hemisphere (Karnath and Zihl, 2003). We have also shown a while back, mimicking the behavior of hemispatial neglect patients (Langner and Eickhoff, 2013), that during drowsy periods, even healthy participants show more errors to the left side of the space in an auditory task (Bareham et al., 2015). However, these alertness-related effects have not been studied in a perceptual decision-making framework which further motivated this study. Hence, we took the opportunity to merge the questions on spatial attention and perceptual decision-making modulated by alertness by implementing an auditory spatial attention task that we developed previously. This paradigm is well defined for this alertness modulation design, and robust and systematic results have been replicated with it. Further, the auditory stimuli can be delivered with eyes closed, and finally it has a simple response option which is appropriate for drowsy participants.

Thus, we designed a study to directly measure tonic alertness and understand its effect on decision-making. Here, we also utilised a recently developed computational method (Jagannathan et al., 2018) to measure alertness directly from EEG, and in combination with multi-level modeling and psychophysics, to understand its effect on behavior. Next, we used a drift-diffusion model (DDM) to parametrise the different elements of the decision-making process, neural decoding for data-driven characterization, and finally, connected the DDM to the neural markers to reveal the compensatory mechanisms of decision-making and spatial attention.

Materials and Methods

Participants

Forty-one healthy human participants (no auditory, neurologic, or psychiatric abnormalities) were recruited. Data from 8 participants were discarded because of technical problems with headphone amplifiers (battery issue was only discovered *post hoc*) and 1 participant for not following task instructions (switching response hand halfway through the experiment). Thus, only data from 32 participants (14 males, age: 24.46 ± 3.72 years old) were considered for further analysis. All participants were self-reported to be right-handed. This was also established by using Edinburgh Handedness Scale (Oldfield, 1971), and each participant had a score of >0 (right-handed) with mean 80.26 ± 23.59. Only easy sleepers (as per self-report) were recruited, and further they were administered with the Epworth Sleepiness Scale (Johns, 1991) on the day of the experiment. Twenty-nine participants had a sleepiness score ≥ 7 (classified as easy sleepers), and 3 of them had a sleepiness score ≥ 4. All participants were asked not to consume any stimulant, such as coffee/tea, before the experiment that day. The study and the experimental protocol were approved by the Cambridge Psychology Research Ethics Committee, and written informed consent was provided by all participants. A monetary compensation of £30 was provided for participation.

Experimental task

Each participant underwent two experimental sessions: alert and drowsy (Figure 1). The alert session lasted ~8 min in duration, with the participants seated upright and lights on. Further, they were instructed to stay awake throughout this session, followed by which the drowsy session was done, which lasted ~1.5-2 h in duration, with the participants reclined to maximum in a chair and lights off to promote drowsiness. Further, they were provided with a pillow for neck support and were allowed to fall asleep. It is critical to note that the intertrial interval in the alert session is 2-3 s, whereas in the drowsy session it is 4-5 s. This increase in intertrial interval, longer duration of session was intended to promote drowsiness in the drowsy session (Kosslyn and Andersen, 1995; Bareham et al., 2014). Before the start of the experiment, the participants were allowed a practice session to become familiar with the task. The trial details for individual session are given below:

Alert session. Participants were presented with 124 complex harmonic tones (guitar chords) that fell on the left or right side of their veridical midline (0°) ranging from −59.31° to 59.31°. These tones were recorded using in-ear microphones in free-field (Bareham et al., 2014). Six tones from −59.31° to −39.26° were presented 2 times each; 12 tones from −35.24° to −1.86° were presented 4 times each. A similar pattern was repeated on the right side with 12 tones from 1.86° to 35.24° presented 4 times each, 6 tones from 39.26° to 59.31° presented 2 times each. The tones in the midline (0°) were presented 4 times, resulting in a total of 124 tones. The order of tones presented was randomized per participant. Further, participants were instructed to keep their eyes closed and respond (as quickly and as accurately as possible) with a button press (using left/right thumb) indicating the location of the tone (left or right). Each trial began after a random interval of 2-3 s; and if the participant did not respond for 5 s, the next trial was started.

Drowsy session. Participants were presented with 740 complex harmonic tones (as above) that fell on the left or right of their veridical midline (0°) again ranging from −59.31° to 59.31°. Six tones from −59.31° to −39.26° were presented 20 times each; 12 tones from −35.24° to −1.86° were presented 20 times each. A similar pattern was repeated on the right side with 12 tones from 1.86° to 35.24° being presented 20 times each, 6 tones from 39.26° to 59.31° presented 20 times each. The tone in the midline (0°) was presented 20 times, resulting in a total of 740 tones. The order of tones was again randomized per participant. Participants were again instructed to keep their eyes closed and respond (as quickly

and as accurately as possible) with a button press (by left/right thumb) indicating the direction of the tone (left or right). Each trial began after a random interval of 4-5 s; and if the participant did not respond for 5 s, the next trial was started. The participants were gently awoken if they did not respond to >3 trials consecutively.

EEG recordings and preprocessing

EEG data were acquired with 128 Ag/AgCl electrodes (Electrical Geodesics) using Cz as the reference electrode. The impedances of all electrodes were kept <100 kΩ (to ensure higher signal-to-noise ratio), and data were acquired at a sampling rate of 500 Hz. EEG data were preprocessed with custom-made scripts in MATLAB (The MathWorks) using EEGLAB toolbox (Delorme and Makeig, 2004). The preprocessing steps are as follows: First, the peripheral electrodes that covered the regions of forehead, cheeks, and neck were removed to reduce artifacts related to eye and muscle movements, thus retaining only 92 channels that covered the scalp. Second, the data were bandpass filtered with zero phase shift between 1 and 40 Hz using hamming windowed-sinc FIR filter and further resampled to 250 Hz. Third, pre-trial and post-trial epochs per trial were created. For the pre-trial epochs, the data were epoched from –4000 to 0 ms before the onset of the stimuli. The pre-trial epochs were created only in the drowsy session and not in the alert session (details below). For the post-trial epochs, the data were epoched from –200 to 800 ms to the onset of the stimuli for both the alert and drowsy sessions. Fourth, the trials that exceeded the amplitude threshold of $\pm 250\,\mu$V were removed in a semiautomatic fashion. Fifth, the bad channels were detected in a two-step fashion: (1) channels are considered bad (zero activity) if channel variance is <0.5; and (2) the normalized power spectrum of the remaining channels was computed and any channel that exceeded the mean power spectrum by ±3 SDs was marked bad. Sixth, to remove further artifacts related to eye-blink and muscle movement, independent component analysis was performed on the channels not marked as bad in the previous step. Independent component analysis components that correspond to artifacts were rejected by manual inspection. Seventh, the bad channels were now interpolated using spherical interpolation. Eighth, the bad trials were detected again using an amplitude threshold of $\pm 250\,\mu$V, and bad electrodes (those exceeding the threshold) in such trials were interpolated in a trial-by-trial fashion. Ninth, the post-trial epochs were rereferenced to the average of all channels (whereas the pre-trial epochs were maintained with the recorded reference, Cz).

Alertness level classification

The preliminary step in both behavioral and neural analysis is to classify trials into "alert" and "drowsy." The data from the pre-trial epochs were used to classify each trial into alert or drowsy. For the alert session, all pre-trial periods were considered to be alert as participants were explicitly instructed to stay awake with short intertrial intervals of 2 s and overall shorter duration of session (both promote wakefulness) and lights switched on, with upright seating. Consequently, none of the participants failed to respond to any of the trials in the alert session, which supported our assumption. In the drowsy session, the participants were allowed to fall asleep with longer intertrial intervals of 4-5 s and lights switched off, with seating reclined to maximum with a pillow for the head support. Hence, several participants failed to respond to some trials in the drowsy session. For each trial in the drowsy session, pre-trial epochs were analyzed using the micro-measures algorithm (Jagannathan et al., 2018). Briefly, the micro-measures algorithm operates on 4 s epochs in a two-step fashion. In the first step, alert(relaxed) trials are separated from the drowsy trials (subdivided into mild and severe) by using a combination of features as follows: variance explained by different frequency band predictors and coherence at different frequency bands (for details, see Jagannathan et al., 2018). For predictor variance, the different features were computed by first generating predictors based on spectral variation in different frequency bands A: 2-4 Hz; B: 8-10 Hz, C: 10-12 Hz; D: 2-6 Hz in the occipital electrodes (E75, E70, E83) and then fitting them per electrode per epoch. For coherence, the frequency bins: δ:[1-4 Hz], theta:[4-7 Hz], alpha:[7-12 Hz], sigma:[12-16 Hz], γ:[16-30 Hz] were used at the occipital: E75 (Oz), E70 (O1), E83 (O2), frontal: E33 (F7), E122 (F8), E11 (Fz), central: E36 (C3), E104 (C4), temporal: E45 (T3-T7), E108 (T4-T8), E102 (TP8), E115, E100 (TP10) sites. These electrode numbers can be identified using the GSN Hydrocel 128 channel map from EGI, and corresponding locations in the standard 10-10 system are given in brackets wherever identified (Luu and Ferree, 2005). In the second step, drowsy(severe) trails were further computed using a combination of grapho-element identification, such as vertex waves, spindles etc. We only used the drowsy(mild) trials for identifying drowsy trials, as the participants usually do not respond under drowsy (severe) trials. We similarly excluded the alert(relaxed) trials in the drowsy session to instead compare the drowsy trials of the drowsy session to all of the trials in the alert session. It should be noted that we could not use the micro-measure algorithm on the alert session as mainly the pre-trial duration was only 2 s, which precludes its application (as 4 s is the recommended for the algorithm). However, none of the participants failed to respond in the alert session as mentioned before. Finally, to cross-validate our assumptions, we performed a *t* test on the distributions of reaction times of the alert versus the drowsy trials per participant. Twenty-eight of the 32 participants significantly differed in reaction time distributions, which is a direct effect of alertness (Ogilvie, 2001), as participants tend to be slower and produce more variable reaction times when drowsy.

The details of this analysis are available at https://github.com/SridharJagannathan/decAlertnessDecisionmaking_JNeuroscience2021/blob/main/Scripts/notebooks/Figure1supplement_RT_persubject.ipynb.

Behavioral analysis

Error proportion. In order to understand how the rate of errors differs across different stimuli (left or right tones) and how it is modulated by alertness levels (alert or drowsy), we performed the following analysis. First, we computed the proportion of errors made by each participant under each alertness level (alert, drowsy) and under each stimulus type (left or right tone). If the total number of trials for any participant under any condition is <5, then the corresponding error proportion (for that condition) is ignored in the analysis. We decided to use multilevel models for this analysis over traditional repeated measures of ANOVA because different participants had different levels of alertness (specifically differing number of alert, drowsy trials per condition). We defined four different multilevel models to understand the modulation of error proportion by state of participant (alert, drowsy) and stimulus (left, right). In the null model, the error proportion depends only on the mean per participant (fixed effect) and the participant ID (random effect). In the second model (state model), the error proportion depends only on the state of the participant (fixed effect) and the participant ID (random effect). In the third model (stimulus model), the error proportion depends only on the stimulus (fixed effect) and the participant ID (random effect). In the fourth model (state-stimulus model), the error proportion depends on a combination of the state of the participant and the stimulus, both used as fixed effects and the participant ID (random effect). These four models were fitted using the lmer function (lmerTest package) in R (Kuznetsova et al., 2017), and the winning model is identified as the one with the highest log-likelihood by comparing it with the null model and performing a likelihood ratio χ^2 test. Finally, the top two winning models were compared against each other using anova function in R (Fox and Weisberg, 2018), to validate whether the winning model (if it is more complex) is actually better than the losing model (if it is simpler). The state-stimulus model emerged as the winning model.

The details of this analysis are available at https://github.com/SridharJagannathan/decAlertnessDecisionmaking_JNeuroscience2021/blob/main/Scripts/notebooks/Figure2a_errorproportion.ipynb.

The different models along with their log-likelihood values are shown in Tables 1 and 2.

The state-stimulus (winning model) was further analyzed with the anova function, and it was found that there was a reliable main effect of both state ($p < 0.001$) and stimulus ($p < 0.001$) on error proportion and also the interaction between state and stimulus also had a reliable effect ($p < 0.01$) on error proportion. Further, we performed *post hoc* tests using Tukey adjustment (for multiple comparisons) to identify differences between pairs that are significant.

Table 1. Model comparison

Model	Parameter	Log-likelihood	p ($>\chi^2$)
Null	Fixed: mean, Random: subj ID	57.55	—
State	Fixed: state, Random: subj ID	63.33	<0.001
Stimulus	Fixed: stimulus, Random: subj ID	65.39	<0.001
State:Stimulus	Fixed: state × stimulus, Random: subj ID	76.39	<0.001

Table 2. Type III ANOVA with Satterthwaite's method of the winning model (state-stimulus)

Model elements	Sum Sq	Mean Sq	NumDF	DenDF	F	p ($>F$)
State	0.23832	0.23832	1	95.08	15.6560	<0.001
Stimulus	0.33053	0.33053	1	93.70	21.7136	<0.001
State:Stimulus	0.13489	0.13489	1	93.70	8.8612	<0.01

Table 3. Model comparison

Model	Parameter	Log-likelihood	p ($>\chi^2$)
Null	Fixed: mean, Random: subj ID	−79.95	—
State	Fixed: state, Random: subj ID	−33.00	<0.001
Stimulus	Fixed: stimulus, Random: subj ID	−79.78	>0.05
State:Stimulus	Fixed: state × stimulus, Random: subj ID	−32.06	<0.001

Table 4. Type III ANOVA with Satterthwaite's method of the winning model (state-stimulus)

Model elements	Sum Sq	Mean Sq	NumDF	DenDF	F	p ($>F$)
State	9.1412	9.1412	1	96	162.463	<0.001
Stimulus	0.0514	0.0514	1	96	0.9138	>0.05
State:Stimulus	0.0557	0.0557	1	96	0.9899	>0.05

Reaction times. In order to understand how the reaction times differ across different stimuli (left or right tones) and how it is modulated by alertness levels (alert or drowsy), we performed a multilevel modeling analysis similar to the analysis on error proportion as above. First, we computed the reaction times of each participant under each alertness level (alert, drowsy) and under each stimulus type (left or right tone). We defined four different multilevel models to understand the modulation of reaction times by state of participant (alert, drowsy) and stimulus (left, right). In the null model, the reaction time depends only on the mean per participant (fixed effect) and the participant ID (random effect). In the second model (state model), the reaction time depends only on the state of the participant (fixed effect) and the participant ID (random effect). In the third model (stimulus model), the reaction time depends only on the stimulus (fixed effect) and the participant ID (random effect). In the fourth model (state-stimulus model), the reaction time depends on a combination of the state of the participant and the stimulus, both used as fixed effects and the participant ID (random effect). The state-stimulus model emerged as the winning model.

The details of this analysis are available at https://github.com/SridharJagannathan/decAlertnessDecisionmaking_JNeuroscience2021/blob/main/Scripts/notebooks/Figure2supplement_RT.ipynb.

The different models along with their log-likelihood values are shown in Tables 3 and 4.

The state-stimulus (winning model) was further analyzed with the anova function, and it was found that there was a reliable main effect of only state ($p < 0.001$) on reaction time.

Subjective midline shifts. The change in subjective midline was quantified by fitting psychometric functions to the responses produced by each participant under alert and drowsy conditions. The proportion of rightward responses for each participant under each stimulus condition from −60° to 60° was fitted with a cumulative normal function using the quickpsy (Linares and López-Moliner, 2016) package in R. In order to evaluate the different parameters involved in the modulation of psychometric functions, we evaluated two different models. The first model was where only the mean of the function shifted for individual participants across alert and drowsy conditions. The second model was where both the mean and the slope shifted across conditions. Model selection was performed using the Akaike Information Criterion; model fits from 9 subjects favored the first model, and 23 subjects favored the second model. Thus, we used the model where both the mean and the slope varied across alert and drowsy conditions. The mean of the cumulative normal function (the point where the curve crosses 0.5 in the y axis) is also referred to as the subjective midline (bias). The subjective midline is the stimulus (angle) at which the participant performs at chance (0.5), which in an ideal world would be closer to the veridical midline (0°). The slope of the cumulative function represents the sensitivity of the system. In general, large variations in the bias point tend to reduce the sensitivity of the system. Further, for performing a paired t test on the change in the parameters across alert and drowsy conditions, we also ignored 13 participants that had a bias point outside ±60° (as the overall stimulus angle can vary only between −60° and 60°) and SD of >30°.

The details of this analysis are available at https://github.com/SridharJagannathan/decAlertnessDecisionmaking_JNeuroscience2021/blob/main/Scripts/notebooks/Figure2c_d_e_psychophysics_biasshift.ipynb.

Drift-diffusion modeling. The different elements of the decision-making process can be teased apart by using the DDM. The parameters of this model include the following: drift rate (v), rate of evidence accumulation, boundary separation distance (a), distance between the two decision boundaries, non-decision time (t), for accounting other processes, such as stimulus encoding (before the start of evidence accumulation process), and response execution (after the end of evidence accumulation). Further, the different sources of bias that can be modeled are as follows: bias point (z), bias in the starting point or drift criterion (dc), a constant factor (slope) added to the drift rate. We implemented the drift diffusion process using a hierarchical DDM (HDDM) (Wiecki et al., 2013) that allows for a hierarchical Bayesian procedure to estimate the model parameters. The principal reason for using such hierarchical procedures is because different participants fall asleep in different ways (differing number of alert and drowsy trials); hence, usage of hierarchical Bayesian procedure allows for robust estimation of model parameters under such limited conditions of trials (Zhang et al., 2016). We used the response of each participant (left or right button press) instead of accuracy (correct or incorrect) to fit the HDDM. Such a procedure is referred to as stimulus coding and allows for robust estimation of sources of bias without being affected by accuracy. In the first step, we decided to identify the sources of bias (with z or dc). Several studies across auditory and visual modalities (Stelmach and Herdman, 1991; Benwell et al., 2014) have shown existence of an initial spatial bias, which is modulated by different factors like time-on-task and alertness levels. Hence, it is important to identify and parametrize the source of this bias to either response driven (changes in z) or stimulus driven (changes in dc) by using model comparison techniques (e.g., χ^2 or based on information criterion) as done in previous studies (Leite and Ratcliff, 2011; White and Poldrack, 2014). For this, we implemented 8 different models that allowed the parameters (z,v) to vary depending on state (alert or drowsy) or stimulus (left or right). Similarly, we implemented 8 different models that allowed the parameters (dc,v) to vary depending on state or stimulus. In each model, 15,000 samples from the posterior distribution were estimated using Markov chain Monte Carlo methods; 5000 samples were further discarded as burn-in to discard the effect of initial values on the posterior distribution estimation. We then choose the best model among the bias models using the one with the lowest deviance information criterion (DIC). DIC allows for computing model accuracy while penalizing for model complexity (Spiegelhalter et al., 2002). The best model among the bias models was where the v varied with state, stimulus and z varied with stimulus alone. In the next step, we used this best model and developed a set of combined models that allows variation in the parameters (a, t) with state or stimulus. We then choose the best model among the four different combined models. The final best model was one where v varied with state, stimulus and z varied with stimulus and a varied with state and t varied with stimulus alone. This final best model checked for model convergence using the Gelman-Rubin statistic. The convergence statistic was computed for 5 different runs and was found to be closer to

0.99 (values closer to 1 but <1.2 indicate convergence) (Spiegelhalter et al., 2002; Gelman et al., 2013).

The details of this analysis are available at https://github.com/SridharJagannathan/decAlertnessDecisionmaking_JNeuroscience2021/blob/main/Scripts/notebooks/Figure3d_k_suppl_hddm.ipynb.

Neural analysis

Decoding. We used multivariate pattern analysis techniques to analyze the divergent patterns in EEG data. Specifically, we used decoding in which patterns of brain activity are analyzed to predict the experimental condition under which it was generated. Traditional ERP analyses rely on using *a priori* identified spatial locations or temporal segments in the data to measure the differences across conditions. However, decoding techniques do not rely on *a priori* definitions and perform much better in detecting differences across experimental conditions (Fahrenfort et al., 2018). Temporal decoding involves using EEG data (X) composed of size: [electrodes × time points × trials] to predict the stimuli presented (Y). The first step consists of fitting an estimator (w) to a subset of the data (X_{train}) to predict a subset of the experimental condition (Y_{train}). The second step involves using this trained estimator on another subset of the data (X_{test}) to predict a subset of the experimental condition (Y_{test}). The third step involves evaluating the performance of this estimator using a validation measure by comparing the prediction ($\hat{Y}_{test}$) with the actual label (Y_{test}).

Estimator construction. First, the EEG data are subjected to a standard scaler (using StandardScaler() from scikit-learn) that removes the mean of the data and scales it by its variance. Second, we used logistic regression to estimate the model parameters for maximally separating the different experimental conditions. Third, we implemented temporal decoding by using the sliding estimator (using SlidingEstimator() from scikit-learn) to fit the logistic regression model per time point.

Cross validation. The EEG data were first downsampled to 100 Hz, and further binary classification was performed between two conditions (left and right stimuli) separately across alert and drowsy conditions per individual participant. As the target of the classification was stimuli being presented, we only considered the trials where the participant made the correct decision. Each participant was considered for classification only if they had at least 25 trials under each condition. Further, five-fold cross validation was performed such that four folds were used for training and the last fold was used as a testing set. The classifier performance was evaluated using area under the curve (AUC) of the receiver-operating characteristic. It is implemented using roc_auc in the sliding estimator function in scikit-learn. When AUC is ~0.5, the classifier performs at chance, while the AUC score of 1 has a very good separability across classes. We computed the AUC–receiver-operating characteristic score per participant as the average of the score across all the cross-validation folds. Further, we smoothed the scores using a 3 point moving average to smooth out spurious fluctuations. In order to identify the reliability of the AUC score at the group level, we performed a cluster permutation test (participants × time points) using MNE (spatio_temporal_cluster_1samp_test) (Gramfort et al., 2013), thus producing p values per time point at the group level, from which time points where we can infer those regions where AUC is reliably different from chance (0.5) at the group level.

Coefficients of patterns. The parameters of the decoding (performed above) are not neurophysiologically interpretable in a straightforward way (Haufe et al., 2014). Hence, the parameters of the backward model (decoding) need to be transformed to produce the forward model. This is done by obtaining the coefficients of the estimator model per participant using the get_coef function from MNE (patterns_). For performing group statistics in electrode space, we used the same cluster permutation-based approach as described earlier.

Decoding of responses. To tease apart the process related to evidence accumulation from motor implementation, we decided to decode the response hand of the participant. The EEG data for the response decoding were created by epoching the data from −800 to 200 ms before the onset of the response from the participant. The response-locked trials were preprocessed in a similar fashion to the stimulus-locked trials. The alertness level for the corresponding response-locked trial was obtained from the labels of the stimulus-locked trial. The decoding and other methods used are similar to the stimulus-locked trials, except that the target of decoding is the response hand being pressed (left or right thumb).

The details of the stimulus decoding are available at https://github.com/SridharJagannathan/decAlertnessDecisionmaking_JNeuroscience2021/blob/main/Scripts/notebooks/Figure4_5_temporaldecodingstimuli.ipynb.

The details of the response decoding are available at https://github.com/SridharJagannathan/decAlertnessDecisionmaking_JNeuroscience2021/blob/main/Scripts/notebooks/Figure6_temporaldecodingresponses.ipynb.

Neuro-behavioral analysis

Regression with DDM. To identify the correlates of the evidence accumulation process, we used the model parameters generated by the DDM (combined best model). First, the ERP data (post-trial epochs) were z-scored per electrode per trial. Second, the ERP data were baseline-corrected with pre-trial data from −200 to 0 ms. Third, the ERP data were averaged every 50 ms per electrode per trial to create 20 time points (−200 to 800 ms) per electrode per trial. Fourth, the ERP data were entered into a trial-by-trial regression with the drift rate using the HDDMRegressor from the HDDM toolbox (Wiecki et al., 2013). The model parameters are allowed to vary as per the combined best model. We estimated the influence of ERP data on the drift rate, as it was the only parameter shown to vary with respect to both the direction of stimulus and the alertness of the participants. Thus, we use drift parameter v as a dependent variable and regressed the same against ERP data as follows:

$$v \sim \beta_0 + \beta_1(\mathrm{ERP})$$

The above equation can be written in patsy form as below.

$$v \sim \mathrm{ERP} : \mathrm{C}(\mathrm{state}, \mathrm{Treatment}(\mathrm{Alert})) : \mathrm{C}(\mathrm{stim}, \mathrm{Treatment}(\mathrm{Right}))$$

Here, the drift rate covaries with the ERP value and depends on a combination of state with a reference value at Alert and of stimulus with a reference value at Right.

The other model parameters are same as in the best model:

$$z \sim \mathrm{stim}, a \sim \mathrm{state}, t \sim \mathrm{state},$$

Here, v represents drift rate, ERP represents z-scored ERP data per trial per time point per electrode, state represents alertness levels (alert or drowsy), and stim represents stimulus types (left or right).

Fifth, the traces were computed per condition (state and stimuli combination). All the regressor models (1840 = 20 × 92 = time points × electrodes) for each participant were checked for convergence using the Gelman-Rubin statistic. The convergence statistic was computed for three different runs and was found to be closer to 0.99 (indicating convergence). Sixth, the differences in drift rate (between left and right stimuli) per time point per electrode were computed in both alert and drowsy condition. This difference represents the discriminability of the electrode in identifying the left and right stimuli at that time point. Thus, this analysis yielded differences in drift rate per electrode, per time point, per condition, per participant. The differences can then be considered similar to the classifier patterns and can be analyzed both in electrode and source spaces. Further, we also computed group-level differences using the cluster permutation techniques described earlier.

The details of this analysis are available at https://github.com/SridharJagannathan/decAlertnessDecisionmaking_JNeuroscience2021/blob/main/Scripts/notebooks/Figure7_hddmregression.ipynb; and comparison of patterns analysis is available at https://github.com/SridharJagannathan/decAlertnessDecisionmaking_JNeuroscience2021/blob/main/Scripts/notebooks/Figure7_8_hddmregressionpatterns_comparison.ipynb.

Source reconstruction of the regression patterns. The coefficients created above can be projected into the source space to infer the brain

regions involved in the pattern activity. Source reconstruction was achieved using a combination of Freesurfer (Fischl, 2012) and MNE. First, the surface was reconstructed using recon-all (Freesurfer) using the default ICBM152 template for the structural MRIs. Next, the Boundary element model was created using make_watershed_bem (MNE). Further, scalp surfaces for the different element boundaries were created using make_scalp_surface (MNE). Second, we performed the registration of the scalp surface with the default EEG channel locations (with fiducials as markers) manually using coregistration (MNE). Third, the forward solution was computed using make_bem_model (MNE). Fourth, to test whether the source reconstruction of the electrode data is accurate, we projected the ERP data of a sample participant into source space and analyzed data from different regions of interest to confirm its validity. The patterns of each participant were then projected into source space in the following manner. First, we computed the noise covariance using the baseline data from −0.2 to 0 ms. Second, we used the forward solution and the noise covariance to create an inverse operator using minimum_norm.make_inverse_operator from MNE. Third, we used the individual pattern per participant and applied the inverse operator on it to produce the source reconstruction of the patterns per participant. For performing group statistics in the source space, we used the same cluster permutation-based approach (after moving them to the fsaverage space) as described earlier.

The details of this analysis are available at https://github.com/SridharJagannathan/decAlertnessDecisionmaking_JNeuroscience2021/blob/main/Scripts/notebooks/Figure9_hddmregressionpatterns_sources.ipynb.

Dataset availability

The raw dataset associated with this study is available at https://doi.org/10.5281/zenodo.5655443.

Results

We organized the results from direct and model-free, to theoretically constrained. Error proportion, reaction times, and subjective midline shifts are described as direct measures to evaluate the effects of alertness, whereas signal detection and DDMs theoretically constrain the interpretation of its parameters to perceptual, central, and motor processes sequentially occurring during perceptual decision-making. We further organized the brain analyses similarly, using multivariate decoding to widely characterize the spatiotemporal neural signatures of the decision; and constrained by the modeled behavioral results, we map the neural dynamics of evidence accumulation in full wakefulness and low alertness. This approach allowed for both open and exploratory neurobehavioral characterization and hypotheses-driven evaluation of the effects of low alertness on perceptual decision-making in spatial attention.

Error proportion modulated by alertness

First, we used multilevel modeling to understand how the errors made by each participant in the auditory tone-localization task were influenced by the stimulus presented (left or right tone) and the state of the participant (alert or drowsy). We defined four different multilevel (linear mixed) models where errors were modulated by various combinations of stimulus and alertness states (see Materials and Methods). The analysis of the variance table of the winning model shows that both alertness ($F_{(1,95.08)} = 15.65$, $p < 0.001$) and stimulus type ($F_{(1,93.70)} = 21.71$, $p < 0.001$) have an effect on error proportion. Further, there was a reliable interaction between alertness levels and stimulus type ($F_{(1,93.70)} = 8.86$, $p < 0.01$). Next, *post hoc* analysis revealed a reliable difference between alert and drowsy conditions for left stimuli ($p < 0.001$), and not for right stimuli ($p = 0.899$). These behavioral results (Fig. 2*A*) replicate the findings of Bareham et al. (2014) in an independent study, task design, alertness measure (and laboratory), reporting an increase in location assignment errors on tones from the left side of the midline when people became drowsy.

Reaction times are modulated by alertness

Second, we aimed to quantify the modulation in the response profiles (reaction times) of individual participants by alertness levels. A paired-sample *t* test with $t_{(31)} = -7.79$, $p < 0.001$ revealed a reliable effect of alertness on reaction time distributions. Further, to this we also used the framework of the multilevel modeling to understand how the reaction times of participants was influenced by the stimulus presented (left or right tone) and the state of the participant (alert or drowsy). We defined four different multilevel (linear mixed) models where errors were modulated by various combinations of stimulus and alertness states (see Materials and Methods). The analysis of the variance table of the winning model shows that only alertness ($F_{(1,96)} = 162.46$, $p < 0.001$) has an effect on reaction times (convergent with the *t* test before). These behavioral results (Fig. 2*B*) converge with the original findings from Hori et al. (1994) indicating slower reaction times under lower levels of alertness, and in agreement to all our previous work (Goupil and Bekinschtein, 2012; Comsa et al., 2019; Canales-Johnson et al., 2020; Noreika et al., 2020).

Subjective midline modulated by alertness

Third, we used psychophysics to quantify the modulation of the subjective midline per participant by alertness levels. For this, we fit a cumulative normal function (see Materials and Methods) to the proportion of rightward responses (per participant) under each stimulus condition from −60° to 60° from the midline under both alert and drowsy periods. The mean of the function referred to as bias is the subjective midline or spatial bias (where participants have 0.5 chance of pressing left or right responses) and the slope represents the sensitivity. Example fits of individual participants are shown in Figure 2*C*. Most participants (Fig. 2*D*) had their bias point shifted to the left (as they became drowsy), indicating more left errors (overestimating the right side of space). A small proportion of participants had bias points shifted to the right. Overall, a paired-sample *t* test $t_{(18)} = 3.53$, $p < 0.01$, revealed a reliable difference in bias points between alert and drowsy periods. Next, we performed a paired-sample *t* test $t_{(18)} = -5.52$, $p < 0.001$, which revealed a reliable difference in slope between alert and drowsy periods. Further, we also plotted (Fig. 2*E*) the mean of the psychometric fits of individual participants to show that the overall subjective midline has shifted to the left at the group level.

Signal detection parameters modulated by alertness

Fourth, we used signal detection theory to understand the factors that modulate decision-making under varying levels of alertness (Fig. 2*F*). d' (sensitivity) showed extreme evidence in favor of the alternative hypothesis (being modulated by alertness) with a Bayes factor = 101,100 while criterion (response bias) only showed anecdotal evidence in favor of the null hypothesis (being not modulated by alertness) with Bayes factor = 1.17. This suggests that internal representations in the brain in terms of sensory/perceptual and noise distributions are modulated by alertness levels. Further, no evidence for response bias also suggests that participants were not arbitrarily pressing right responses for uncertain stimuli with drowsiness.

To summarize, the behavioral results hint that the first two stages of perceptual and evidence accumulation processes are

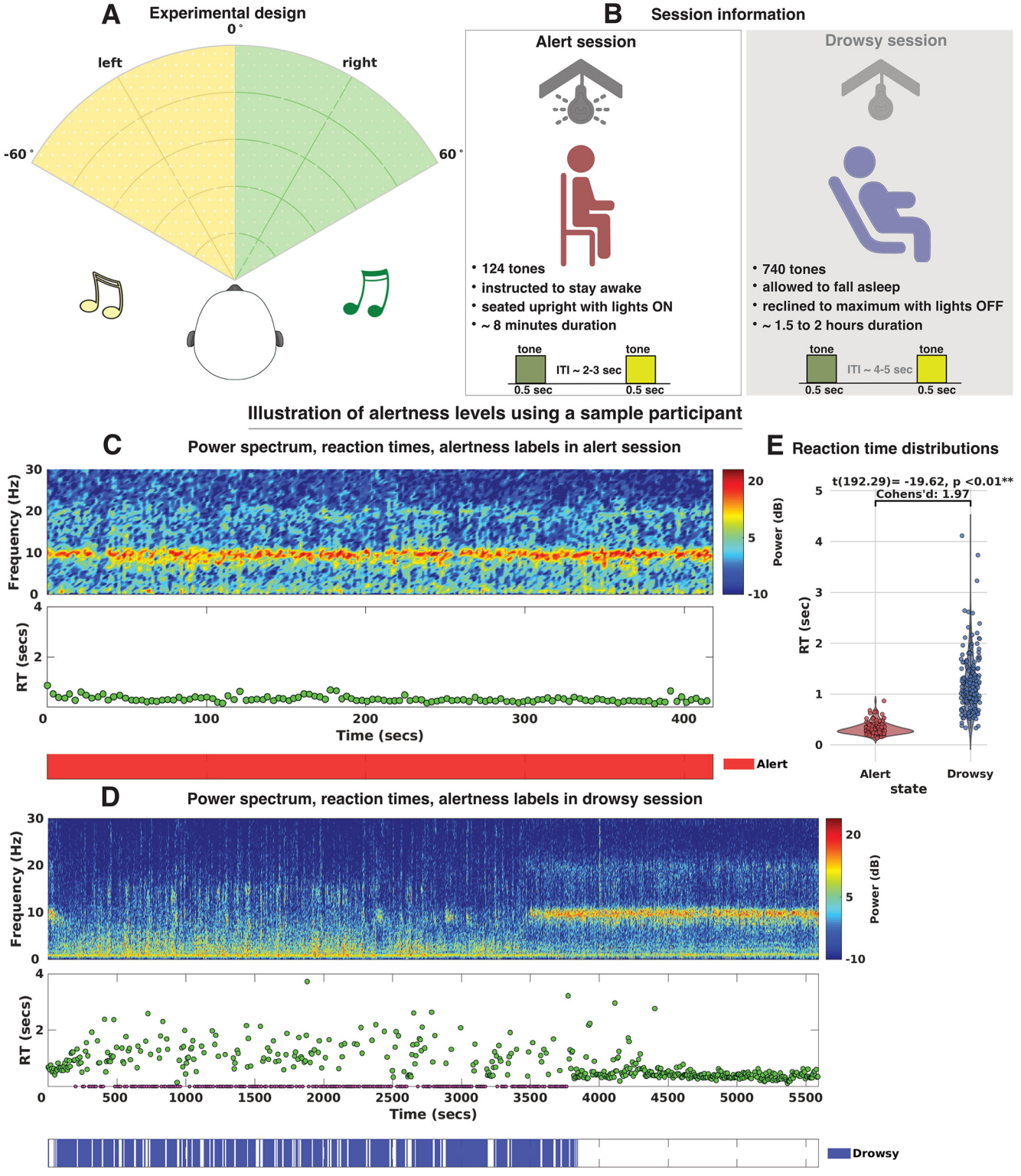

Figure 1. ***A***, Auditory spatial attention task. Participants had to localize the direction of auditory tones coming from left and right side of the midline. ***B***, Session details. Each participant underwent an alert and drowsy session. In the alert session of ~8 min in duration, participants are instructed to stay awake and seated upright with lights on. The shorter intertrial interval of 2-3 s and shorter duration of the session ensured that none of the participants failed to respond in any of the trials. In the drowsy session of ~1.5-2 h in duration, participants are allowed to fall asleep with the seat reclined to maximum with a pillow for head support. The longer intertrial interval of 4-5 s and longer duration of the session ensured that most participants became drowsy. ***C***, ***D***, Alert and drowsy trial identification. All the trials in the alert session are considered to be alert (124), whereas among the 740 trials in the drowsy session, we used the micro-measures algorithm (Jagannathan et al., 2018) and divided the pre-trial periods into different categories, among which we choose the mild drowsy trials. Here we can see that, in the drowsy session, this sample participant failed to respond several times (purple dots in RT plot) and the drowsy trial labels coincide in the nearby periods, whereas in the alert session the participant systematically responds. ***E***, Cross-validation of alert and drowsy trial labels per participant. For each participant, we then performed a *t* test comparing the distribution of reaction times of alert versus drowsy trials and found that, for 28 of 32 participants, the distributions reliably differed, validating the approach (Jagannathan et al., 2018).

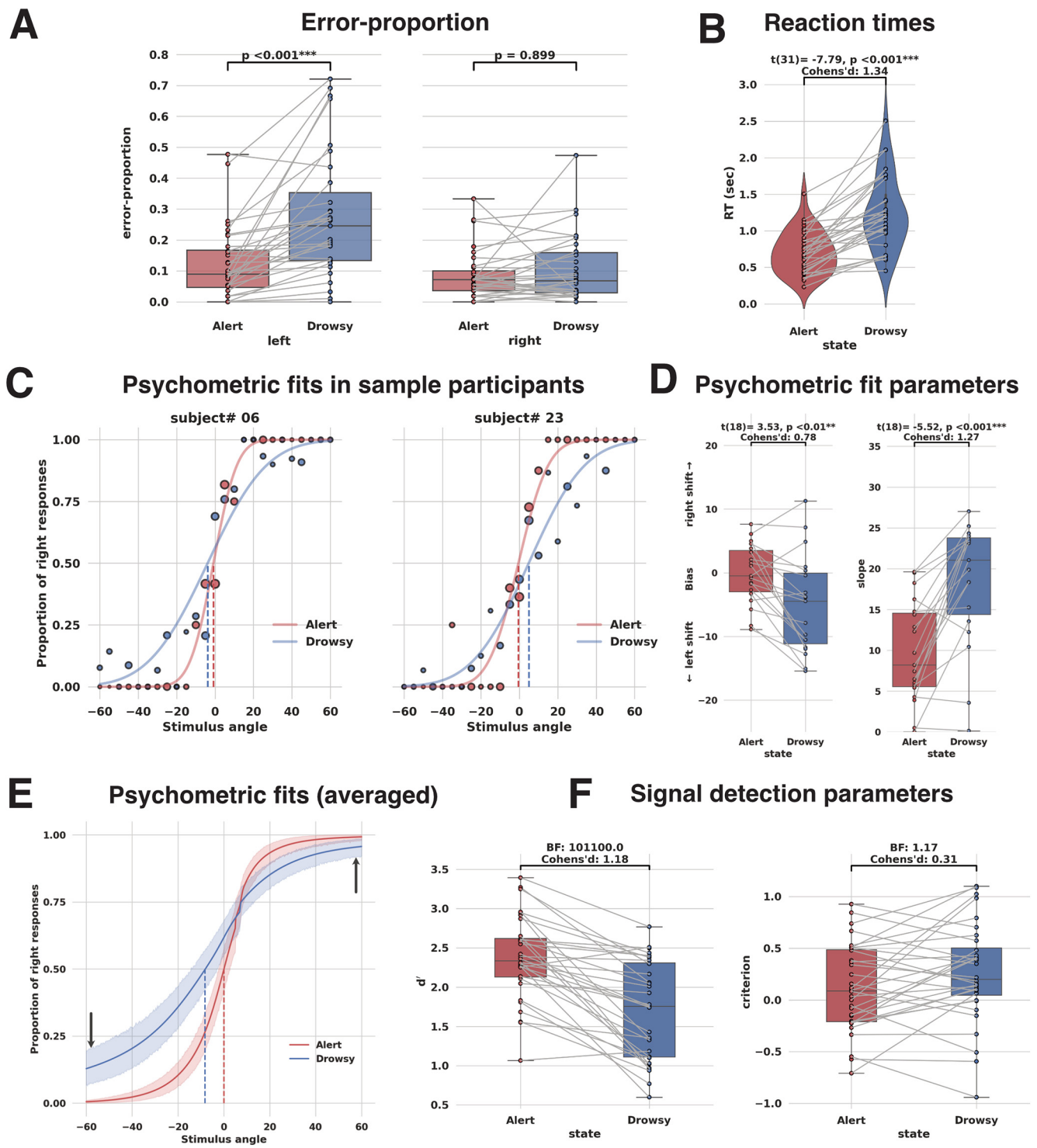

Figure 2. Behavioral analysis. ***A***, Proportion of errors committed in alert and drowsy periods across left and right stimuli. Multilevel modeling reveals that error rates depend on stimulus and state of the participant. *Post hoc* tests indicate that error proportion is reliably modulated by alertness but only for left stimuli. ***$p < 0.001$. ns, Not significant (or not reliable). Error bars indicate SEM. ***B***, Mean reaction times for individual participants. Reaction times are variable and slower under drowsy conditions; further, a paired-samples *t* test indicates reliable difference ($p < 0.001$) in reaction times across alert and drowsy periods. ***C***, Example fits of two different participants are shown. For each participant under each condition (alert, drowsy), the proportion of rightward responses was fitted to the stimulus angle varying from −60° to 60°. The size of the dots represents the normalized (per condition) number of trials under each angle. Here, we notice that the bias point (dotted line) shifts toward the left side as the participant becomes drowsy. In other words, as the participant becomes drowsy, they overestimate the right side of space. For another participant, we notice the opposite effect. ***D***, Spatial bias. Slope parameter per participant (from psychometric fits). Bias level shifts toward the left side (indicating more left errors) for most participants. Negative bias values indicate shifts in the subjective midline toward the left, and positive values indicate shift toward the right. Further, a paired-sample *t* test indicates reliable difference ($p < 0.01$). Slope values of the psychometric fits also increased as participants became drowsy, indicating shallower slopes. Further, a paired-sample *t* test indicates reliable difference ($p < 0.001$). ***E***, Group-level psychometric fits indicate the shift in subjective midline (dotted lines). Shaded regions represent CI bounds. Arrows indicate a gap in the asymptotes at −60° compared with 60° between alert and drowsy state, further evidence of inattention to the left side. ***F***, Signal detection analysis shows that *d′* (sensitivity) is strongly modulated by alertness compared with c (criterion) using Bayes factor.

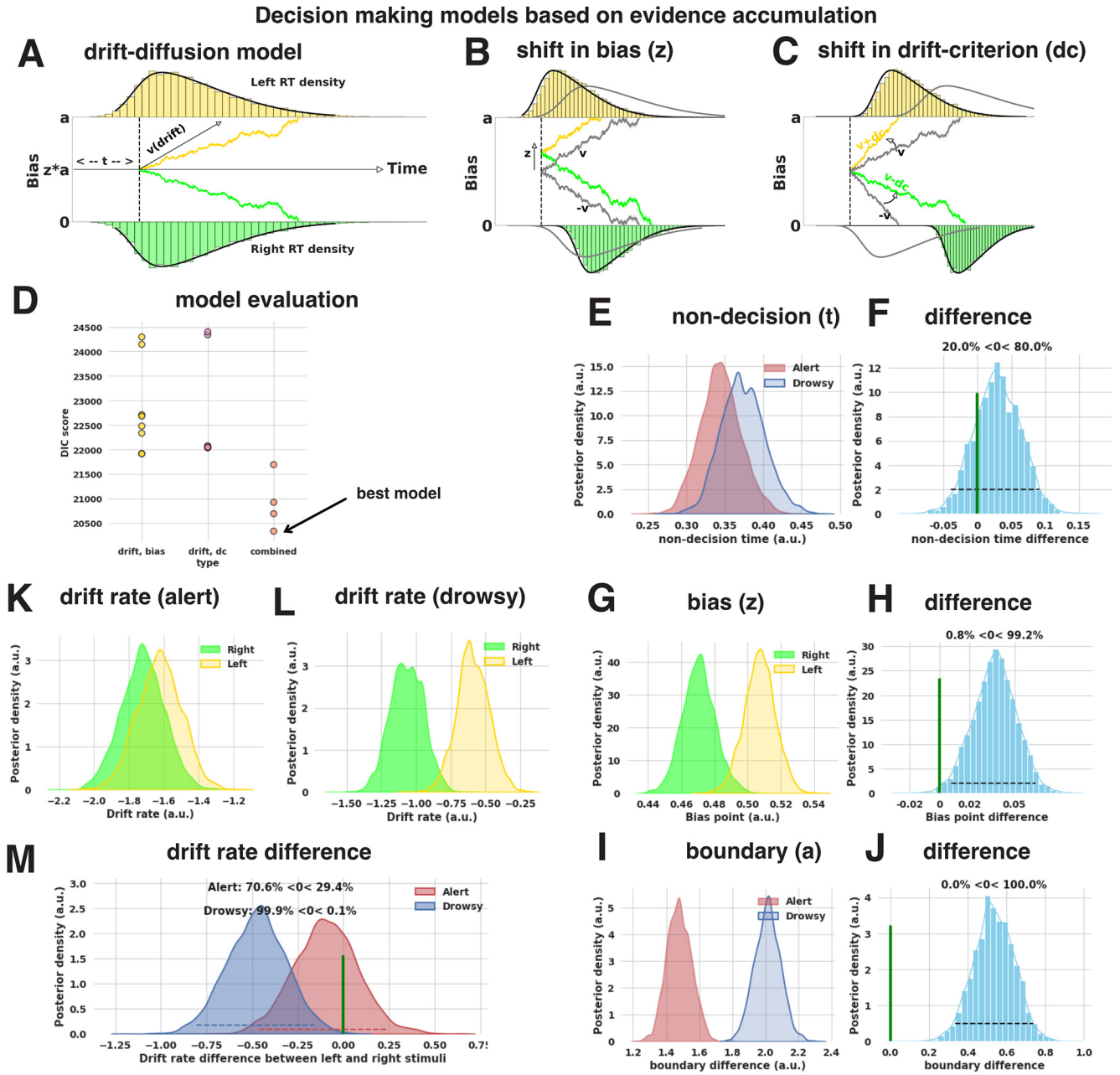

Figure 3. Evidence accumulation models. ***A***, DDM accounts for the reaction time distributions of responses across left and right stimuli (stimulus coding). *v*(drift) indicates evidence accumulation rate, *a* indicates the boundary separation, *z* indicates the bias point (usually $z = 0.5$ for unbiased responses), and *t* indicates non-decision time composed of stimulus encoding and response execution. ***B***, ***C***, Changes in response distributions can be explained by different sources of bias. Shift in starting point (*z*) or constant offset added to drift rate (drift criterion). Gray lines indicate unbiased condition. ***D***, In the first step, the appropriate source of bias (either *z* or dc) was identified. In our case, the source of bias was identified as *z* based on the lowest DIC. Further, this bias (*z*) was combined with different variations in *t*, *a*, and *v*, and the best model with the lowest DIC was identified (see Materials and Methods). ***E***, ***F***, Posterior densities of *t* in the best model, and their differences indicate there is no reliable change (based on proportion of posterior overlap, here 20.0%) across alert and drowsy periods. ***G***, ***H***, Posterior densities of *z* in the best model, and their differences indicate there is a reliable change (based on proportion of posterior overlap, here 0.8%) across left and right stimuli. ***I***, ***J***, Posterior densities of *a* in the best model, and their differences indicate there is a reliable change (based on proportion of posterior overlap, here 0%) across alert and drowsy periods. ***K***, ***L***, Posterior densities of *v* for left and right stimuli across alert and drowsy periods in the best model. ***M***, Differences in the posterior densities of changes in drift rate indicate strong evidence (overlap reduces to 0.1% from 29.4%) in favor of change in drift rate across stimuli in the drowsy period compared with alert periods.

affected by decreasing alertness and that the final stage of motor implementation (response bias/criterion) may be less affected.

Alertness modulates SSM parameters of evidence accumulation

Next, we aimed to quantify the different elements of the decision-making process using drift-diffusion modeling. The DDM captures the optimal procedure involved in performing a 2-alternative forced choice task under sequential sampling framework. It assumes that the observer accumulates evidence for one or other alternative in every time step (Ratcliff et al., 2016), until integrated evidence reaches a threshold to decision (Fig. 3*A*). The localization of tones to the left and right side of space is essentially a 2-choice task with the participant always forced to make a decision on the location of the tone. The model was implemented with a hierarchical Bayesian procedure using

HDDM (see Materials and Methods). For the HDDMs, we fit the response of each participant instead of accuracy. This procedure is referred to as stimulus coding, allows for the testing of several decision-making parameters, and is critical to uncover different sources of bias (de Gee et al., 2017).

We examined models with different sources of bias: starting point (z) (Fig. 3*B*) or constant slope (dc) (Fig. 3*C*) and identified the best model as one with the lowest DIC (see Materials and Methods). The best model showed that drift rate (v) varied according to state (alert or drowsy) and stimulus (left or right), bias point (z) varied according to stimulus (left or right) but not state, non-decision time (t) varied according to state (alert or drowsy), and decision threshold (a) varied according to state (alert or drowsy). This furthers the claim that the changes in alertness place a higher burden in the evidence accumulation process (drift rate), and less on the motor implementation or stimulus encoding of the task (non-decision time). The best model was then analyzed for differences in posterior densities of parameters. For this purpose, we used a Bayesian estimate, which is more informative and avoids the arbitrary choices of significance level implemented for specific statistical tests used by the frequentist-based methods (Kruschke, 2013).

In the best model, the proportion of posterior overlap in the non-decision time (between alert and drowsy states) was 20.0% (Fig. 3*F*). This indicates that the non-decision time was not reliably different between the different states. Next, the proportion of posterior overlap in the bias point (between left and right stimuli) was 0.8% (Fig. 3*H*). This indicates that the bias point was reliably different between the different stimuli. Next, the proportion of posterior overlap in the boundary (between alert and drowsy states) was 0% (Fig. 3*J*). This indicates that the boundary was reliably different between the different states. Importantly, only the drift rate varied with respect to both the stimuli and the state, suggesting that the difference in evidence accumulation (indicated by the drift rate) is responsible for the difference in error rates between left and right stimuli in the low alertness state, as shown in the previous analyses. Here, the proportion of posterior overlap (between left and right stimuli) in the drift rate for alert trials was 29.4% and reduced to 0.1% for drowsy trials (Fig. 3*M*). Thus, the drift rate (evidence accumulation rate) was reliably different between left and right stimuli on drowsy trials compared with the alert trials.

To summarize, the behavior modeling results hint that only the central evidence accumulation process (indicated by drift rate) is affected by decreasing alertness, whereas processes responsible for perceptual encoding and response execution may not be modulated.

Spatial and temporal signatures involved in spatial localization across alert and drowsy periods

Here, we were interested in identifying the neural signatures involved in the performance of this task. For this purpose, decoding involves identifying the stimulus (Y, left or right tone) presented from the EEG data (X). This process involves the identification of the W (classifier weights) that can produce the transformation, $Y_t = W_t X_t$ where t represents time (Fig. 4*A*,*B*). The performance of the classifier (W) is evaluated by training and testing the data at each time point (t) using AUC as measure. In Figure 4*C*, the shaded region represents those periods reliably decoded ($p < 0.05$) (for more details, see Materials and Methods).

We found that, when participants were alert, the reliable decoding of stimuli (Fig. 4*D*) started at 160 ms after the stimulus and lasted until 730 ms (cluster permutation, $p < 0.05$) with mean AUC of 0.57. The peak discriminatory power was at 280 ms (AUC = 0.60). The average AUC between 200 and 300 ms was 0.58 ± 0.007, $p < 0.05$, between 300 and 400 ms was 0.57 ± 0.002, $p < 0.05$. However, when the participants became drowsy, the decoding of stimuli (Fig. 4*E*) shifted to 440 ms after the stimulus was presented and lasted until 740 ms (reliable with cluster permutation, $p < 0.05$) with mean AUC of 0.53. The peak discriminatory power was at 590 ms (AUC = 0.55). The average AUC between 440 and 500 ms was $M = 0.53 \pm 0.001$, $p < 0.05$, between 500 and 590 ms was $M = 0.54 \pm 0.003$, $p < 0.05$. This suggests that the processes related to the discrimination between left and right stimuli under drowsy conditions may cease to be directly informative to the decision in the early processes of sensory encoding and would only start later, at ~400 ms, to show neural differentiation.

Further to this, the lower discriminatory power points to a potentially less efficient (lower decodability, longer time duration, higher variability) process of central evidence accumulation, or to a different neural implementation of the processes during low alertness.

Next, we plotted the coefficients of the classifier patterns (derived from classifier weights W) in the scalp electrode space for further neurophysiological interpretation. We decided to compare the classifier patterns across early (<300 ms) and later (>400 ms) time periods. To compare patterns in the early time periods across alert and drowsy periods, we plotted the same for every 40 ms between 180 and 420 ms in Figure 4*F*. For the alert periods, the pattern between 180 and 220 ms indicates a strong involvement of signal in the frontocentral electrodes, whereas in the corresponding time periods under drowsy, the pattern seems to have shifted to more frontal electrodes, although its contribution may be minimal as it was not reliably decodable. Under alert periods, the pattern shifts to more posterior regions (centroparietal electrodes in the right side of the scalp) between 220 and 260 ms, whereas under drowsy the pattern stays in the frontal electrodes itself, still not reliably decodable in the unconstrained voltage decoding. Further, from 260 to 300 ms, the pattern shifts to more parietal and occipital sites under alert periods and is only weakly parietal in the drowsy periods.

The comparison of the classifier patterns across alert and drowsy periods (in early time periods) reveals different topographies that point to a clear differential processing of information that would further map onto shifted perceptual and central evidence accumulation stages of cognitive processing (Sigman and Dehaene, 2005), possibly affecting the central accumulation. To compare patterns in the later time periods across alert and drowsy periods, we plotted the same for every 40 ms between 420 and 660 ms in Figure 4*G*. Particularly, the patterns in the alert periods have a lower frontal activity and higher posterior activity, whereas in the drowsy periods, the activity in both the frontal and posterior sites is much more localized, although decodability is overall lower. Although only suggestive, this change in the decodability intensity and distribution suggests a delayed processing dynamics and/or a change in the way of processing as alertness decreases.

The descriptive analysis of the classifier patterns indicates differences between alert and drowsy periods. To establish the spatial and temporal signatures of such differences, we performed a cluster permutation test and identified regions where activity patterns in alert periods are different from drowsy periods. This analysis resulted in the identification for four clusters (Fig. 5).

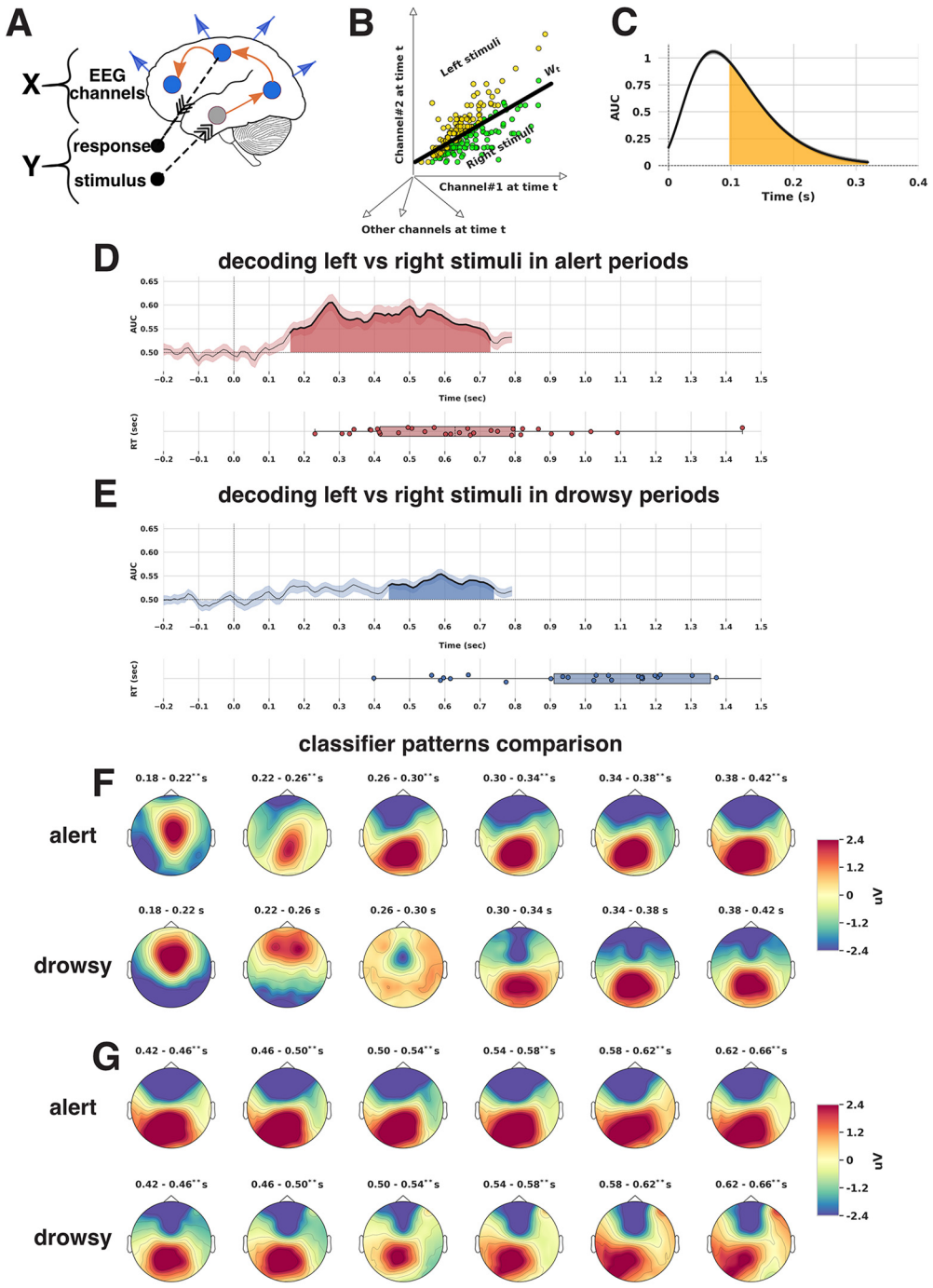

Figure 4. Temporal decoding (stimuli). ***A***, Decoding consists of identifying Y (stimuli) from X (EEG). The model thus consists of $Y_t = W_t X_t$, where t represents time and W_t represents transformation (classifier weights). Here, the predicted output Y consists of categorical labels (left/right tone) predicted from brain activity (X). ***B***, Classifier weights W_t are determined by the optimal separation of different classes (here left, right stimuli). ***C***, Decoding performance is assessed using the AUC where shaded regions represent reliably different time periods ($p < 0.05$). ***D***, ***E***, AUC under alert and drowsy periods, where the classifier was trained to discriminate between targets of left and right stimuli. Shaded regions represent time periods with reliable ($p < 0.05$) discriminatory power, computed with a cluster-based permutation test. The mean reaction times (RT) of participants are plotted below. ***F***, Comparison of coefficients of classifier patterns in the early time periods. The early time periods highlight topographical differences in the frontal, posterior parietal, and central electrodes. ***G***, Comparison of coefficients of classifier patterns in the later time periods. The later time periods highlight topographical differences in the frontal and central electrodes. **Reliably discriminatory in the corresponding period in temporal decoding.

1. Cluster #1 (alert activity > drowsy activity): indicates early periods (150-330 ms), where activity is concentrated in parietal, central, posterior electrode sites. These spatial patterns are likely to be involved in early perceptual/evidence accumulation processes during the alert periods, as the majority of responses only start occurring from 400 ms onward.
2. Cluster #2 (alert activity > drowsy activity): indicates later periods (430-650 ms), where activity is concentrated in occipital, parietal, central, posterior electrode sites. These spatial patterns are difficult to interpret as the reaction times overlap with the corresponding time periods. Hence, this decoding pattern could be an amalgamation between central evidence accumulation and motor implementation processes.

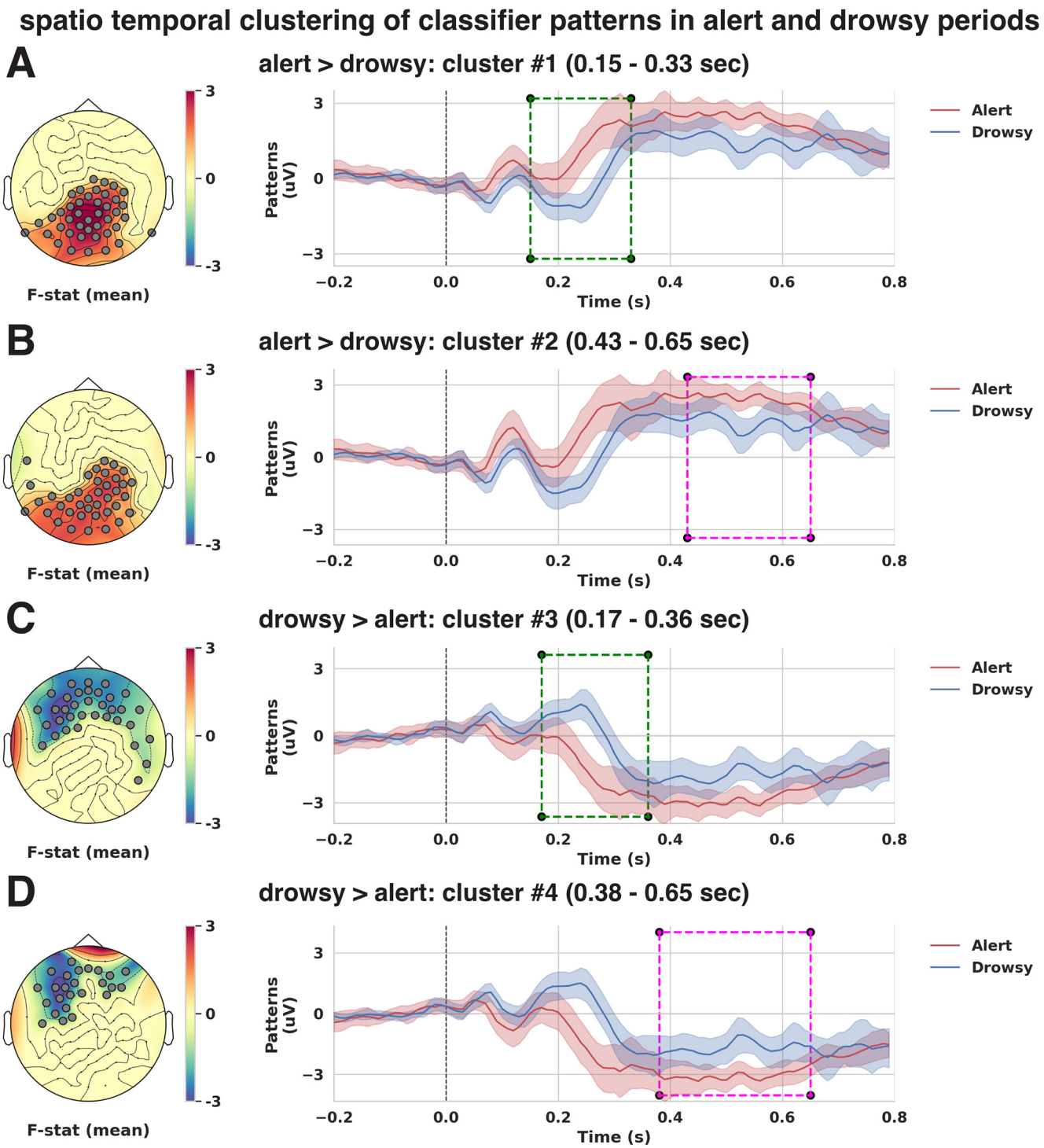

Figure 5. Classifier pattern differences. To identify differences between the classifier patterns in Figure 4*F*, *G*, we performed spatiotemporal clustering using a permutation test. ***A***, Cluster #1 indicates early periods (150-330 ms after stimulus) where alert activity is higher than drowsy periods. ***B***, Cluster #2 indicates later periods (430-650 ms after stimulus) where alert activity is higher than drowsy periods. In terms of spatial locations, the early and later clusters differ in right parietal sites, central, middle electrode sites. ***C***, Cluster #3 indicates early periods (170-360 ms after stimulus) where drowsy activity is higher than alert periods. ***D***, Cluster #4 indicates later periods (380-650 ms after stimulus) where drowsy activity is higher than alert periods. In terms of spatial locations, the early and later clusters differ in left frontal sites, middle electrode sites.

3. Cluster #3 (drowsy activity > alert activity): indicates early periods (170-360 ms), where activity is concentrated in frontal electrode sites. These spatial patterns are likely to be involved in early perceptual/sensory encoding processes during the drowsy periods, as the majority of responses only start occurring from 900 ms onward. The temporal neurodynamics show delayed patterns in drowsy compared with awake.
4. Cluster #4 (drowsy activity > alert activity): indicates later periods (380-650 ms), where activity is concentrated in left frontal electrode sites. These spatial patterns are likely to be involved in central evidence accumulation-related processes. However, it is difficult to interpret as the corresponding time periods during alert mildly overlap with response-related activity.

To summarize, these results indicate differences in spatial patterns related to early sensory/evidence accumulation-related process (cluster #1, cluster #3) across alert and drowsy periods. The next step is to identify and tease apart motor preparation-related processes occurring during later time periods.

Spatial and temporal signatures of motor implementation across alert and drowsy periods

In classic cognitive processing model frameworks, motor implementation occurs after the central evidence processes, when information of the decision is routed to the premotor network, this is assumed to be mostly; a serial process. We preprocessed the EEG data now locked to responses (see Materials and Methods) and decoded the response hand itself (regardless of the stimulus presented). These response-related patterns thus would depict information related to the motor implementation process regardless of the decision related processes.

The decoding performance: AUC (Fig. 6*A*,*B*) starts ramping up from −210 ms (alert), −150 ms (drowsy) from the response time, and increases when the button is actually pressed at 0 s, reaching the peak soon after. In both cases, awake and drowsy, the neural decoding results last until 190 ms. These results are in line with motor implementation-related processes commonly reported ∼200 ms before the actual motor response, gradually ramping up to produce the response itself. It is also interesting to note that the AUC for alert is always higher than drowsy, indicating less variability in neural concerted activity; leading to better classifier performance without time span differences, this may indicate a more efficient motor implementation in the awake state.

To establish the spatial and temporal signatures of differences in motor-related processes, we performed a cluster permutation test of classifier patterns and identified regions where activity patterns in alert periods are different from drowsy periods. This analysis resulted in the identification of two clusters (Fig. 6*C*,*D*).

1. Cluster #1 (alert activity > drowsy activity): indicates periods (−220 to 190 ms), where activity is concentrated in premotor, parietal, posterior electrode sites.
2. Cluster #2 (drowsy activity > alert activity): indicates periods (−350 to 190 ms), where activity is concentrated in premotor, frontal electrode sites.

The existence of a single cluster (in time) across both alert and drowsy periods further indicates that motor-related processes do not necessarily vary in time with modulations in alertness levels. Furthermore, for both alert and drowsy periods, the start of the decoding happens during similar time periods at ∼−200 ms and lasts until similar time periods ∼190 ms.

In summary, these results indicate that motor preparation-related processes are similar during both alert and drowsy trials, suggesting that this process may not be critical to the changes in decision-making in low alertness compared with evidence accumulation-related processes. Although the efficiency of the implementation may be lower in drowsy, this could be because of differences in signal-to-noise with alertness or to changes in the neural implementation of the action itself.

The above analysis related to decoding of stimuli, and responses indicate that most likely only central evidence accumulation-related processes are modulated by alertness. However, the decoding analysis in the late clusters could be confounded by response-related processes occurring during alert periods. Hence, we devised the next step of the analysis where we use parameters derived from the drift diffusion modeling to understand how different elements of the evidence accumulation are represented in the neural domain. This analysis is determined by the DDM as a mathematical implementation of decision-making theory, and it guides neural exploration to capture the brain dynamics echoes of the evidence accumulation process.

Neural signatures of evidence accumulation of decision-making modulated by alertness

To take advantage of the information gained by the drift diffusion modeling, we decided to capture the neural implementation of the evidence accumulation parameters in the decision-making process, and how it might differ in wakefulness and low alertness periods. We specifically aimed at capturing the change in the neurobehavioral dynamics of the evidence accumulation process in the awake and drowsy periods. To establish this, we developed a novel method based on the drift-diffusion analysis shown earlier. We used the best model (from the drift diffusion analysis earlier) and computed trial-by-trial influence of a brain covariate (ERP) on the DDM parameters (see Materials and Methods). Further, we compute the proportion of the overlap of the posterior distributions of the trace obtained for both left and right stimuli separately under alert and drowsy conditions (Fig. 7*A*). This analysis is repeated for each participant; and we obtain regression patterns, similar to the classifier patterns but guided by the drift rate, per participant.

Next, we plot the regression patterns in alert and drowsy periods. The patterns in the alert periods (Fig. 7*C*,*D*) indicate that the topography focuses initially in the frontocentral electrodes (150-250 ms), which then shifts to centroparietal electrodes (250-350 ms), similar to the classifier analysis (decoding patterns from Fig. 4*F*,*G*). The patterns in the drowsy periods (Fig. 7*C*,*D*) indicate that the topography initially focuses on the frontal electrodes (though weaker compared with alert periods) in the interval from 150 to 250 ms. Further, the patterns shift to more central electrodes (again weaker compared with alert periods) in the interval from 250 to 350 ms.

The descriptive analysis of the regression patterns indicates differences between alert and drowsy periods. To establish the spatial and temporal signatures of such differences, we performed a cluster permutation test and identified regions where activity patterns in alert periods are different from drowsy periods. This analysis resulted in the identification of two clusters (Fig. 8).

1. Cluster #1 (alert activity > drowsy activity): indicates early periods (125-275 ms), where activity is concentrated in parietal and central electrode sites. These spatial patterns are likely to be involved in early perceptual and evidence accumulation processes.
2. Cluster #2 (drowsy activity > alert activity): indicates early periods (175-325 ms), where activity is concentrated in frontal/central electrode sites. These spatial patterns are likely to be involved in early perceptual/sensory encoding processes during the drowsy periods.

These analyses indicate spatial/temporal regions where the alert and drowsy periods differ in terms of sensory encoding and central evidence accumulation-related processes. Furthermore, we have also teased apart these differences from motor-related processes by directly using a parameter (drift rate) from the hierarchical drift diffusion modeling.

Alertness modulates frontoparietal cortical neural patterns in perceptual decision-making

Next, we performed an exploratory analysis to identify the putative neural sources of these differences (Fig. 9) using a source

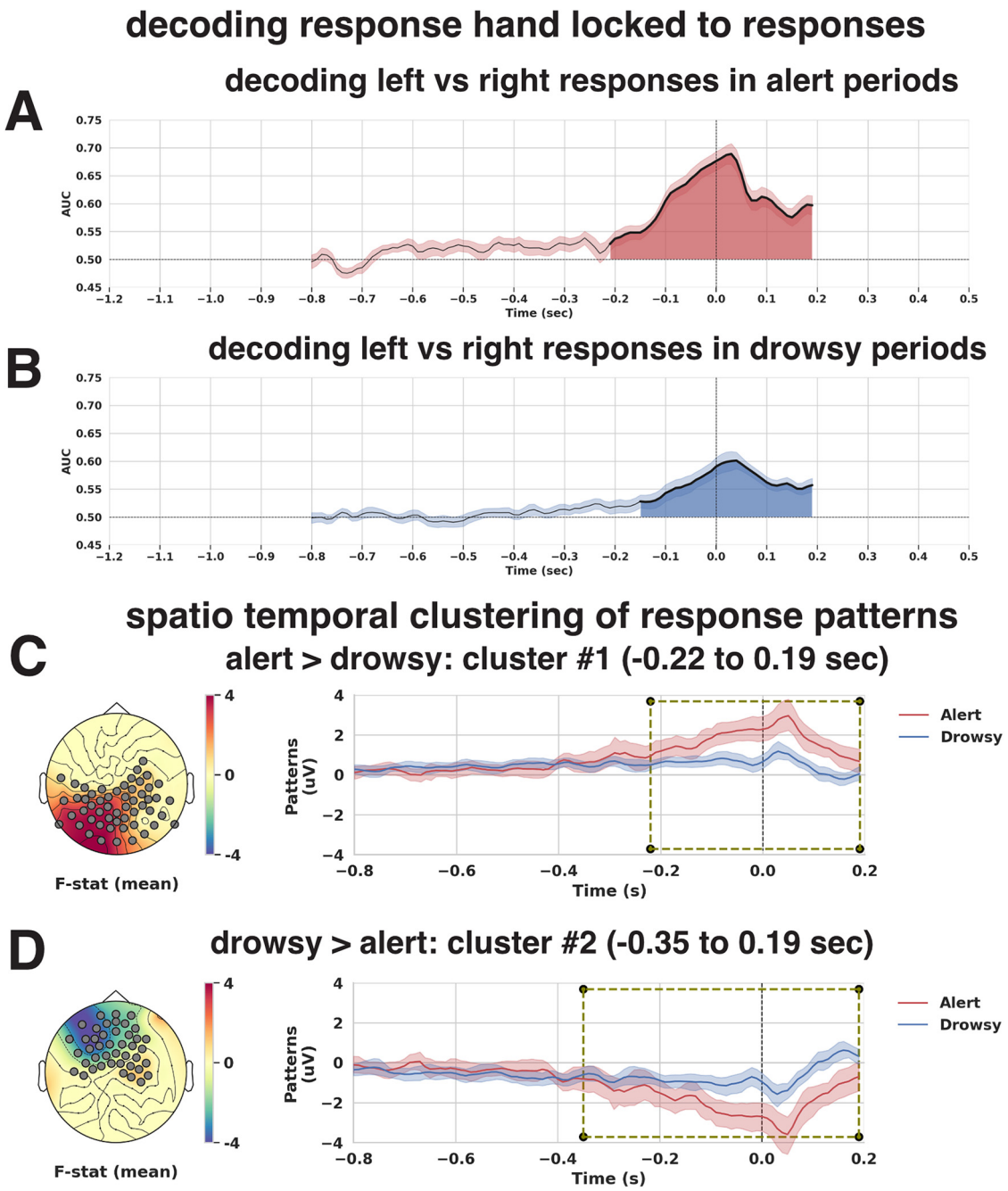

Figure 6. Temporal decoding (responses). To identify differences in motor preparation (response-related), we decoded the left and right button press events regardless of stimuli presented. ***A***, ***B***, AUC under alert and drowsy periods, where the classifier was trained to discriminate between targets of left and right button presses. Shaded regions represent time periods with reliable ($p < 0.05$) discriminatory power. The time point of 0 corresponds to the actual button press event. The ramp up of the AUC under both conditions starting from 210 ms (alert), 150 ms (drowsy) before the actual response indicates the ability of the decoder to detect neural signatures related to responses. Spatiotemporal clustering of differences in classifier patterns produces two clusters with similar time periods in contrast to the clusters (with early and later time periods) produced by stimuli-related classifier patterns. ***C***, Cluster #1 indicates periods (−220 to 190 ms) where alert activity is higher than drowsy periods. ***D***, Cluster #2 indicates periods (−350 to 190 ms) where drowsy activity is higher than alert periods. In terms of spatial locations, the clusters differ in frontal, central, middle, parietal electrode sites. The presence of a single cluster with similar time periods across alert and drowsy periods indicates that motor-related processes start appearing at similar time periods and hence do not change with modulations in alertness levels.

reconstruction procedure to project the classifier patterns of the different clusters back to their neural sources separately. In the source space, we performed cluster permutation tests to identify where in the cortex the activity in alert periods is higher than in drowsy periods. We used the actual value of the source activity (instead of absolute values), as we are interested in the distance between the two different patterns and not in overall activity levels.

1. Cluster #1: This cluster corresponds to regions where activity in alert periods is higher than drowsy periods. These regions are putative locations for early sensory, evidence accumulation-related processes in alert periods. The analysis reveals regions (inferior parietal lobule) previously associated with the ventral attention network (Corbetta and Shulman, 2011; Yeo et al., 2011) in the right hemisphere. The analysis further reveals

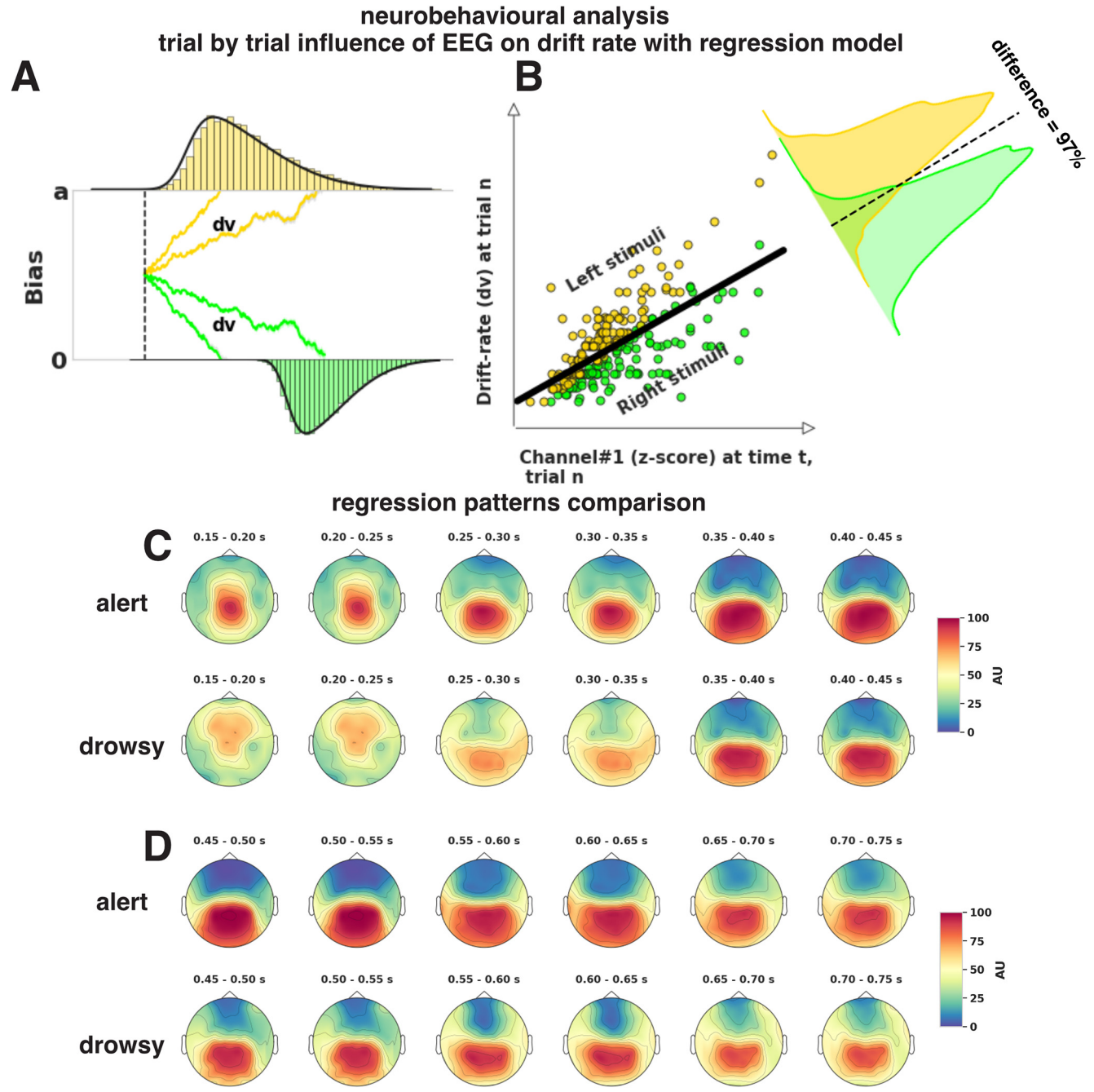

Figure 7. Regression patterns. ***A***, ***B***, EEG data (*z*-scored and averaged per 50 ms) was regressed against drift rate (*v*), the difference in the posterior of regression rate was quantified per electrode per time point per participant. ***C***, ***D***, Mean regression patterns in alert and drowsy periods projected in electrode space show a classic centrofrontal to parietal progression from 150 to 750 ms. The early time periods highlight topographical differences in the frontal, middle, central parietal electrodes.

regions (superior parietal) that are part of the dorsal attention network (Corbetta and Shulman, 2011; Yeo et al., 2011) and central processing of flexible information (Fedorenko et al., 2013).

2. Cluster #2: This cluster corresponds to regions where activity in drowsy periods is higher than alert periods. These regions are putative locations for early sensory-related processes in drowsy periods. The analysis reveals regions (superior temporal gyrus, inferior frontal gyrus, supramarginal gyrus, transverse temporal, temporoparietal, frontoparietal, middle frontal gyrus) regions in the right hemisphere also associated with the ventral attention network (Corbetta and Shulman, 2011; Yeo et al., 2011).

To summarize, these results indicate that, during alert periods, the early sensory/central accumulation-related processes (until 300 ms from stimulus presentation) are located in the regions corresponding to the dorsal attention network (which is specialized for spatial attention). For the drowsy periods, the early sensory encoding-related processes (until 300 ms from stimulus presentation) are located in the regions corresponding to the frontoparietal, ventral attention network, further during later periods (after 300 ms) evidence accumulation-related process are located in the regions corresponding to frontoparietal network. This indicates that frontoparietal regions of the brain are further recruited for the late decision-making processes implemented in the drowsy periods, pointing to a cortical

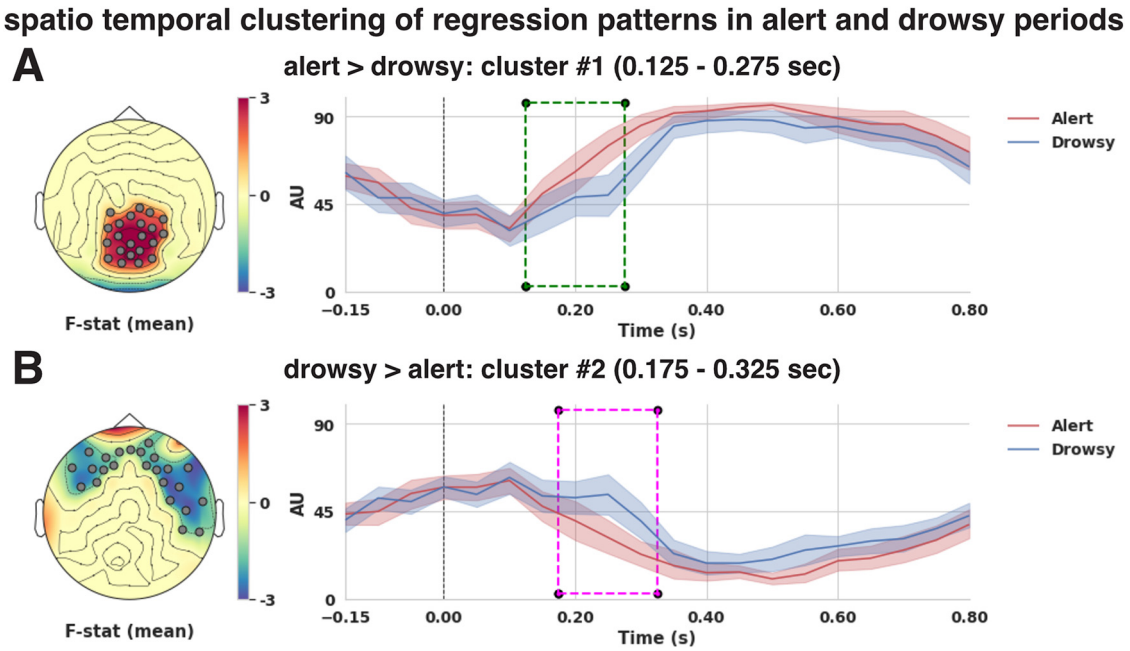

Figure 8. Regression pattern differences. Spatiotemporal clustering of differences in regression patterns shown in Figure 7*C*, *D* between alert and drowsy periods. ***A***, Cluster #1 indicates early periods (125-275 ms after stimulus) where alert activity is higher than drowsy periods. In terms of spatial locations, cluster #1 identifies electrodes in right parietal sites, central, middle electrode sites. ***B***, Cluster #2 indicates early periods (175-325 ms after stimulus) where drowsy activity is higher than alert periods. In terms of spatial locations, cluster #2 identifies electrodes in left/right frontal sites, right middle electrode sites.

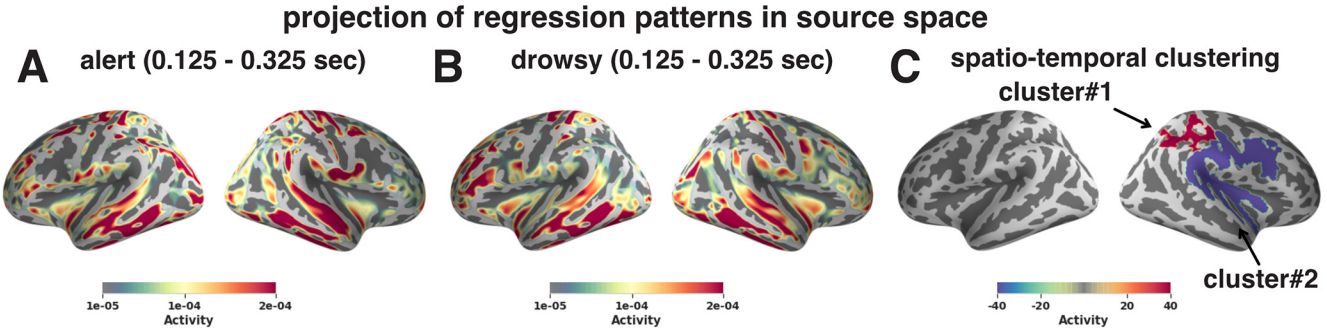

Figure 9. Regression patterns projected into source space. To identify the putative regions/networks in the brain related to perceptual decision-making and its modulation by alertness, we projected the regression patterns in Figure 8 to source space. ***A***, Average regression patterns in the alert periods (125-325 ms) projected into source space. ***B***, Average regression patterns in the drowsy periods (125-325 ms) projected into source space. ***C***, Cluster #1 (alert > drowsy) identifies differences in regions related to the dorsal and ventral attention network in the right superior and inferior parietal regions, respectively. Cluster #2 (drowsy > alert) reveals differences in regions related to the ventral attention network in the superior-temporal, frontoparietal regions.

network reconfiguration in the evidence accumulation between normal and low alertness periods.

Discussion

In this study, we characterize cognitive and neural dynamics of perceptual decision-making while participants are falling asleep. First, we established, using multilevel modeling, that errors for left-sided stimuli (compared with right) increased as participants become drowsy, in convergence with Bareham et al. (2014) but with a different study design, analysis methods, and participants sample. Further, we fitted the proportion of rightward responses of individuals and identified the subjective midline, showing that shifts to the left (more rightward responses) as people become drowsy. These echo line-bisection studies (Jewell and McCourt, 2000), showing that healthy individuals bisect lines to the left of the veridical midline, and further support meta-analysis studies suggesting rightward shift in attention with lower levels of alertness (Chandrakumar et al., 2019). Additional studies (Benwell et al., 2014) have also identified possible neural origins of such bias as task-independent activity in the ventral attention network; however, they did not examine whether trial-to-trial alertness of individuals was modulated and how the different aspects of the decision-making process were affected. Several studies (Corbetta and Shulman, 2011) have shown that activity in the ventral attention network interacts with the alertness system, and that low alertness, as shown directly here, could be the root cause.

Next, using signal detection theory (SDT), we found that sensitivity (d') had strong evidence of modulation by low alertness, whereas criterion showed anecdotal evidence in favor of no modulation, complementing early deprivation studies in vigilance tasks (Deaton et al., 1971). This suggests that the sensory/perceptual representations have indeed been modulated by alertness, and that participants were not arbitrarily pressing more rightward responses (in the face of uncertain stimuli) as alertness

decreases. Further, using the SSM framework, we showed that in the best model, only the drift rate was reliably modulated by both alertness and stimuli, whereas starting point was only affected by stimuli (reliable), and boundary (reliable) and non-decision time (not reliable) were affected by alertness. This shows that alertness indeed differentially modulates evidence coming from the left side of space compared with the right. Decision-making studies in the visual modality (Smith and Ratcliff, 2009) have shown that drift rates are closely related to the strength of stimulus encoding, partially affected by attentional strength and evidence accumulation to a decision threshold. Further studies have also shown neural correlates of such parameters in the EEG (O'Connell et al., 2012; Nunez et al., 2017) and its relationship with stimuli strength. Hence, we interpret the effect of alertness modulation on drift rate as acting specifically on spatial attention affecting the stimulus encoding, as well as in central processes of evidence accumulation. Finally, it is important to compare the parameters of the SDT with the DDM (Jun et al., 2021). The changes in sensitivity (d') in SDT could be directly related to the changes in the boundary parameter (a) and drift rate (v) in the DDM. Here the changes in d′ are in agreement with both v and a as both are shown to be modulated by alertness levels. The changes in criterion (c) in the SDT correspond to sources of bias and they could be originating from the stimulus: corresponding to drift criterion (dc) in the DDM or originating from the response: corresponding to starting point (z) in the DDM. With the evaluation of competing models we show that models with z outperforms the models with dc, further z varies only stimulus direction (left or right) and is not modulated by alertness. This agrees with previous studies showing an initial spatial bias (Benwell et al., 2013; Learmonth et al., 2015) even before any experimental modulation (like time on task or alertness). Here the evidence for the modulation of z in the DDM across stimuli direction and not alertness levels agrees with the non-modulation of criterion in the SDT across alertness levels.

Next, using time-multivariate decoding, we showed that under alert conditions the decoding started early, at 160 ms and lasted until 730 ms; however, under drowsy conditions, this was delayed to 440 ms and lasted until 740 ms. This ~280 ms delay may indicate that, under lower alertness, the brain requires a longer time to decipher, or process, the direction of stimuli as suggested by slower reaction times and a change in the drift rate, or alternatively, that the neural code in this window is too noisy to be captured by this neural decoding. Furthermore, the overall strength of decoding was systematically higher in alert than drowsy, suggesting that the brain processes responsible for decision-making are less variable under the alert compared with the drowsy condition, or that there is less efficient decision processing during low alertness (for an account on sleep deprivation on cognition, see Killgore, 2010).

The different neural time clusters potentially point to a first stage of information encoding and second of central evidence accumulation (Kelly and O'Connell, 2015) that others have mapped to perceptual/central decision processes (Sigman and Dehaene, 2008). If that is the case, the first neural signal cluster in drowsy (cluster #3 in Fig. 5*C*), showing changes in the spatial pattern and a lack of reliable decoding may be interpreted as less efficient encoding and transfer of information in low alertness or may be using different network dynamics that are not captured by the direct time-voltage decoding. The second cluster (cluster #4 in Fig. 5*D*), more similar between states, may signal a lower efficiency of central evidence accumulation, as it happens around the time the central decision process occurs in cognitive control (Ho et al., 2009). Furthermore, the second window of processing may also show part of the motor implementation processes at least for the awake condition (cluster #2 in Fig. 5*B*), where the responses overlap for several participants (Fig. 4*D*). The overlapping processes from ~400 ms in awake, a mixture of central evidence accumulation and motor implementation of the decision, depending on the participant, are easily dissociated when drowsy, when the motor plan is implemented ~500 ms later (~900 ms). This is complemented by the response-locked analyses that seem to confirm a common motor implementation, and it further guides the subsequent analysis.

Further analyses of the classifier patterns suggested specific signatures of early perceptual and late central cognitive processes. In the alert condition, the early pattern (180-220 ms) indicates activity over frontocentral electrodes, further shifting to more central and parietal sites later on. In the drowsy condition, the pattern initially starts at frontal sites (though not strong enough to be decoded) and shifts to central and parietal sites, later on from 380 ms onward. Thus, the formation of central, parietal patterns (possibly related to the first stage of encoding, evidence accumulation) takes longer or starts later in drowsy periods compared with alert. The spatial and temporal distribution of this centroparietal decoding pattern resembles both a classic P2 and early P3, which has been dubbed as the build-to-threshold signal (Twomey et al., 2015), and the centroparietal positivity, a more specific signal of evidence accumulation (Loughnane et al., 2016), respectively. To disambiguate the neural implementation of the evidence accumulation, we developed a novel method using regression patterns that identified differences in drift rate across alert and drowsy periods and further tested neural differences between alertness conditions.

Cluster #1 (alert>drowsy) showed activity in inferior parietal source regions that resemble the patterns of the ventral attention network. Although we cannot directly differentiate between early perceptual encoding and central accumulation processes, this cluster most likely corresponds to both in the alert periods. This part of the process of the spatial decision shows the early involvement of regions that have been linked, in several studies (Shulman et al., 2010; Dietz et al., 2014), to lesions in the inferior parietal lobule resulting in egocentric neglect. Furthermore, lower activity in the ventral attention network was also reported for neglect patients suffering from deficits in arousal (Corbetta and Shulman, 2011). This agrees with the higher activity observed in the regression patterns for the alert periods compared with the drowsy periods of lower alertness. Further, it also revealed regions in superior parietal that have been associated with the dorsal attention network (Shulman et al., 2010; Dietz et al., 2014). Again, these regions most likely correspond to the central evidence accumulation that is directly involved in evaluation of the spatial attention information.

Cluster #2 (drowsy>alert) showed activity in the transverse temporal, superior temporal gyrus, temporoparietal junction, frontoparietal regions (inferior frontal, middle frontal gyrus) in the right hemisphere that can also be considered part of the ventral attention network. Several studies (Heilman et al., 1987; Corbetta et al., 2005) have reported lesions in the right ventral frontal cortex in patients suffering from both arousal related deficits and neglect to the right side of space. The highlighting of these regions in our study indicates that they are different from the alert periods and their higher activity in the regression patterns points to a potential source of spatial neglect caused by alertness deficits, which is similar to that observed in patient and studies in healthy volunteers with causal manipulation (Paladini

et al., 2017). This could be dissociated in further studies, either with lesion meta-analysis or with virtual lesions in normal volunteers as we recently suggested (Bareham et al., 2018). We think this cluster corresponds to a combination of sensory encoding and evidence accumulation in the drowsy periods, highlighting an early cortical reconfiguration of the evidence accumulation process.

When participants are fully alert, we think the information is processed initially by the ventral attention network, followed by the dorsal (specialized in spatial attention), whereas when participants are drowsy the ventral attention network, although disproportionately affected in the right hemisphere (Heilman et al., 1987; Corbetta et al., 2005; Corbetta and Shulman, 2011), is still involved in sensory encoding and early evidence accumulation processes. This reconfiguration in the ventral attention network is further propagated in the next stage, the dorsal attention network. This second part of the decision closely tallies with the proposal by Corbetta and colleagues to account for spatial neglect found in stroke patients suffering from lesions in right-hemispheric regions. But further, this network shows temporal and spatially extended recruitment of the parietal and frontopolar cortices to compensate for the direct effects of lower alertness, and that reconfiguration of the brain networks to relatively maintain performance may be a common and expected mechanism (Canales-Johnson et al., 2020).

As we lose consciousness, the neural system responsible for decision-making adapts to the internal challenge of decreasing arousal and shows its resilience, exerting homeostatic regulations at the cognitive level to maintain performance. The attention and wakefulness fluctuations experienced in humans (and characterized in other animals) are common during the day; and they are not only dependent on the circadian and sleep-wake regulation pressure (Borbély et al., 2016), but also on genetic, epigenetic, environmental, and life history factors that shape the alertness aspects of attention as well as the alertness aspect of arousal (Bekinschtein et al., 2009a; Mitchell, 2020).

From a decision-making perspective, we have added a missing level of description by characterizing possible mechanisms of resilience of the neurocognitive processes elicited by decreases in tonic alertness. When moving from fully alert to a lower alertness state the brain tries to recruit and expand evidence accumulation-related processes to frontoparietal regions instead of temporoparietal regions, consistent with an increase in cognitive demand proposed by the Multiple Demand system (Duncan, 2010). We interpret that the neural reconfiguration occurring in the transition from fully awake to decreased alertness brings different neural dynamics and changes the nature of the noise in the brain, forcing the cognitive system to exchange information differently. We put forward that low alertness negatively impacts the efficiency of the evidence accumulation processes, and differentially impacts performance, and the response of the system is to compensate by extending its neural processes in time and space to attempt to maintain performance. These findings highlight the neural dynamics of decision-making when the external world remains unaltered, physical evidence held constant, but the internal milieu fluctuates exerting a modulatory influence on the cognitive decision-making systems that caused them to reconfigure to solve the task at hand.

Transition of consciousness in the near-awake to light-decrease of alertness is emerging as a model for internally caused interactions (Tagliazucchi and Laufs, 2014; Comsa et al., 2019; Canales-Johnson et al., 2020; Noreika et al., 2020; Song and Tagliazucchi, 2020). With lesion and pharmacological challenges, neuropsychology and cognitive neuroscience have tried to define the necessary and sufficient brain networks, areas and dynamics of the brain to implement cognition, revealing compensation, reconfiguration, and plasticity (Adolphs, 2016; Valero-Cabré et al., 2017; Yeung et al., 2018). Semicausal effect of the internal interference exerted by the relative independence of the arousal system on the cognitive process paves the way for the use of wakefulness, alertness, and arousal challenges in a principled manner, adding new tools for cognitive brain research. Cognitive neuroscience uses models, correlational and causal methods to reach consensus about the underlying mechanism of thought (Krakauer et al., 2017). Here, we have followed a theoretically motivated question about perceptual decision-making systems, using behavioral modeling to understand the system, but at the same time causally modulating the neural networks with alertness decreases to uncover the mechanisms of brain function.

References

Adolphs R (2016) Human lesion studies in the 21st century. Neuron 90:1151–1153.

Bareham CA, Tristan A, Bekinschtein SK, Manly ST (2015) Does left-handedness confer resistance to spatial bias? Sci Rep 5:9162.

Bareham CA, Georgieva SD, Kamke MR, Lloyd D, Bekinschtein TA, Mattingley JB (2018) Role of the right inferior parietal cortex in auditory selective attention: an rTMS study. Cortex 99:30–38.

Bareham CA, Manly T, Pustovaya OV, Scott SK, Bekinschtein TA (2014) Losing the left side of the world: rightward shift in human spatial attention with sleep onset. Sci Rep 4:5092.

Bekinschtein T, Dehaene S, Rohaut B, Tadel F, Cohen L, Naccache L (2009a) Neural signature of the conscious processing of auditory regularities. Proc Natl Acad Sci USA 106:1672–1677.

Bekinschtein T, Cologan V, Dahmen B, Golombek D (2009b) You are only coming through in waves: wakefulness variability and assessment in patients with impaired consciousness. Prog Brain Res 177:171–189.

Benwell CS, Thut G, Learmonth G, Harvey M (2013) Spatial attention: differential shifts in pseudoneglect direction with time-on-task and initial bias support the idea of observer subtypes. Neuropsychologia 51:2747–2756.

Benwell CS, Harvey M, Thut G (2014) On the neural origin of pseudoneglect: EEG-correlates of shifts in line bisection performance with manipulation of line length. Neuroimage 86:370–380.

Borbély AA, Daan S, Wirz-Justice A, Deboer T (2016) The two-process model of sleep regulation: a reappraisal. J Sleep Res 25:131–143.

Buchanan L, O'Connell A (2006) A brief history of decision making. Harv Bus Rev 84:32–41. 132.

Canales-Johnson A, Beerendonk L, Blain S, Kitaoka S, Ezquerro-Nassar A, Nuiten S, Fahrenfort J, van Gaal S, Bekinschtein TA (2020) Decreased alertness reconfigures cognitive control networks. J Neurosci 40:7142–7154.

Chandrakumar D, Keage HA, Gutteridge D, Dorrian J, Banks S, Loetscher T (2019) Interactions between spatial attention and alertness in healthy adults: a meta-analysis. Cortex 119:61–73.

Comsa IM, Bekinschtein TA, Chennu S (2019) Transient topographical dynamics of the electroencephalogram predict brain connectivity and behavioural responsiveness during drowsiness. Brain Topogr 32:315–331.

Corbetta M, Shulman GL (2011) Spatial neglect and attention networks. Annu Rev Neurosci 34:569–599.

Corbetta M, Kincade MJ, Lewis C, Snyder AZ, Sapir A (2005) Neural basis and recovery of spatial attention deficits in spatial neglect. Nat Neurosci 8:1603–1610.

Deaton M, Tobias JS, Wilkinson RT (1971) The effect of sleep deprivation on signal detection parameters. Q J Exp Psychol 23:449–452.

de Gee JW, Colizoli O, Kloosterman NA, Knapen T, Nieuwenhuis S, Donner TH (2017) Dynamic modulation of decision biases by brainstem arousal systems. eLife 6:e23232.

Delorme A, Makeig S (2004) EEGLAB: an Open Source toolbox for analysis of single-trial EEG dynamics including independent component analysis. J Neurosci Methods 134:9–21.

Dietz MJ, Karl J Friston, Friston JB, Roepstorff A, Garrido MI (2014) Effective connectivity reveals right-hemisphere dominance in audiospatial perception: implications for models of spatial neglect. J Neurosci 34:5003–5011.

Duncan J (2010) The multiple-demand (MD) system of the primate brain: mental programs for intelligent behaviour. Trends Cogn Sci 14:172–179.

Fahrenfort JJ, van Driel J, van Gaal S, Olivers CN (2018) From ERPs to MVPA using the Amsterdam Decoding and Modeling Toolbox (ADAM). Front Neurosci 12:368.

Fedorenko E, Duncan J, Kanwisher N (2013) Broad domain generality in focal regions of frontal and parietal cortex. Proc Natl Acad Sci USA 110:16616–16621.

Fischl B (2012) FreeSurfer. Neuroimage 62:774–781.

Fox J, Weisberg S (2018) An R companion to applied regression. Thousand Oaks, CA: SAGE.

Gelman A, Carlin JB, Stern HS, Dunson DB, Vehtari A, Rubin DB (2013) Bayesian data analysis, Ed 3. Boca Raton, FL: CRC.

Gold JI, Shadlen MN (2007) The neural basis of decision making. Annu Rev Neurosci 30:535–574.

Goupil L, Bekinschtein TA (2012) Cognitive processing during the transition to sleep. Arch Ital Biol 150:140–154.

Gramfort A, Luessi M, Larson E, Engemann DA, Strohmeier D, Brodbeck C, Goj R (2013) MEG and EEG data analysis with MNE-Python. Front Neurosci 7:267.

Haufe S, Meinecke F, Görgen K, Dähne S, Haynes JD, Blankertz B, Bießmann F (2014) On the interpretation of weight vectors of linear models in multivariate neuroimaging. Neuroimage 87:96–110.

Heilman KM, Bowers D, Valenstein E, Watson RT (1987) Hemispace and hemispatial neglect. In: Advances in psychology (JeannerodM, ed), pp 115–150. Elsevier.

Hori T, Hayashi M, Morikawa T (1994) Topographical EEG changes and the hypnagogic experience. In: Sleep onset: normal and abnormal processes. (Ogilvie RD, Harsh JR eds), pp 237–253. American Psychological Association.

Ho TC, Brown S, Serences JT (2009) Domain general mechanisms of perceptual decision making in human cortex. J Neurosci 29:8675–8687.

Hull JT, Wright KP Jr, Czeisler CA (2003) The influence of subjective alertness and motivation on human performance independent of circadian and homeostatic regulation. J Biol Rhythms 18:329–338.

Jagannathan SR, Ezquerro-Nassar A, Jachs B, Pustovaya OV, Bareham CA, Bekinschtein TA (2018) Tracking wakefulness as it fades: micro-measures of alertness. Neuroimage 176:138–151.

Jewell G, McCourt ME (2000) Pseudoneglect: a review and meta-analysis of performance factors in line bisection tasks. Neuropsychologia 38:93–110.

Johns MW (1991) A new method for measuring daytime sleepiness: the Epworth Sleepiness Scale. Sleep 14:540–545.

Jun EJ, Bautista AR, Nunez MD, Allen DC, Tak JH, Alvarez E, Basso MA (2021) Causal role for the primate superior colliculus in the computation of evidence for perceptual decisions. Nat Neurosci 24:1121–1131.

Karnath HO, Zihl J (2003) Disorders of spatial orientation. In: Neurological disorders, pp 277–286. Elsevier.

Kelly SP, O'Connell RG (2015) The neural processes underlying perceptual decision making in humans: recent progress and future directions. J Physiol Paris 109:27–37.

Killgore WD (2010) Effects of sleep deprivation on cognition. Prog Brain Res 185:105–129.

Knowles JB (1993) Sleep, sleepiness and performance (Monk TH, ed). Wiley.

Kosslyn S, Andersen MR (1995) Frontiers in cognitive neuroscience. Cambridge, MA: MIT Press.

Krakauer JW, Ghazanfar AA, Gomez-Marin A, MacIver MA, Poeppel D (2017) Neuroscience needs behavior: correcting a reductionist bias. Neuron 93:480–490.

Kruschke JK (2013) Bayesian estimation supersedes the t test. J Exp Psychol Gen 142:573–603.

Kuznetsova A, Brockhoff PB, Christensen RHB (2017) LmerTest package: Tests in linear mixed effects models. J Stat Softw 82:1–26.

Langner R, Eickhoff SB (2013) Sustaining attention to simple tasks: a meta-analytic review of the neural mechanisms of vigilant attention. Psychol Bull 139:870–900.

Learmonth G, Thut G, Benwell CS, Harvey M (2015) The implications of state-dependent tDCS effects in aging: behavioural response is determined by baseline performance. Neuropsychologia 74:108–119.

Leite FP, Ratcliff R (2011) What cognitive processes drive response biases? A diffusion model analysis. Judgment and Decision Making 6:651–687.

Linares D, López-Moliner J (2016) Quickpsy: an R package to fit psychometric functions for multiple groups. The R Journal 8:122–131.

Link SW, Heath RA (1975) A sequential theory of psychological discrimination. Psychometrika 40:77–105.

Loughnane GM, Newman DP, Bellgrove MA, Lalor EC, Kelly SP, O'Connell RG (2016) Target selection signals influence perceptual decisions by modulating the onset and rate of evidence accumulation. Curr Biol 26:496–502.

Luu P, Ferree T (2005) Determination of the HydroCel Geodesic Sensor Nets' average electrode positions and their 10–10 international equivalents. Technical Note 1–11.

McGinley MJ, Vinck M, Reimer J, Batista-Brito R, Zagha E, Cadwell CR, Tolias AS, Cardin JA, McCormick DA (2015) Waking state: rapid variations modulate neural and behavioral responses. Neuron 87:1143–1161.

Mitchell KJ (2020) Innate: how the wiring of our brains shapes who we are. Princeton, NJ: Princeton UP.

Noreika V, Andrés CJ, Amy J, Aurina A, Justin K, Srivas C, Bekinschtein TA (2020) Wakefulness fluctuations elicit behavioural and neural reconfiguration of awareness. bioRxiv 155705. doi: https://doi.org/10.1101/155705.

Nunez MD, Vandekerckhove J, Srinivasan R (2017) How attention influences perceptual decision making: single-trial EEG correlates of drift-diffusion model parameters. J Math Psychol 76:117–130.

O'Connell RG, Dockree PM, Kelly SP (2012) A supramodal accumulation-to-bound signal that determines perceptual decisions in humans. Nat Neurosci 15:1729–1735.

O'Connell RG, Shadlen MN, Wong-Lin KF, Kelly SP (2018) Bridging neural and computational viewpoints on perceptual decision-making. Trends Neurosci 41:838–852.

Ogilvie RD (2001) The process of falling asleep. Sleep Med Rev 5:247–270.

Oldfield RC (1971) The assessment and analysis of handedness: the Edinburgh Inventory. Neuropsychologia 9:97–113.

Paladini RE, Müri RM, Meichtry J, Nef T, Mast FW, Mosimann UP, Nyffeler T, Cazzoli D (2017) The influence of alertness on the spatial deployment of visual attention is mediated by the excitability of the posterior parietal cortices. Cereb Cortex 27:233–243.

Ratcliff R, Smith PL, Brown SD, McKoon G (2016) Diffusion decision model: current issues and history. Trends Cogn Sci 20:260–281.

Robertson IH, Mattingley JB, Rorden C, Driver J (1998) Phasic alerting of neglect patients overcomes their spatial deficit in visual awareness. Nature 395:169–172.

Shulman GL, Pope DL, Astafiev SV, McAvoy MP, Snyder AZ, Corbetta M (2010) Right hemisphere dominance during spatial selective attention and target detection occurs outside the dorsal frontoparietal network. J Neurosci 30:3640–3651.

Sigman M, Dehaene S (2005) Parsing a cognitive task: a characterization of the mind's bottleneck. PLoS Biol 3:e37.

Sigman M, Dehaene S (2008) Brain mechanisms of serial and parallel processing during dual-task performance. J Neurosci 28:7585–7598.

Smith PL, Ratcliff R (2009) An integrated theory of attention and decision making in visual signal detection. Psychol Rev 116:283–317.

Song C, Tagliazucchi E (2020) Linking the nature and functions of sleep: insights from multimodal imaging of the sleeping brain. Curr Opin Physiol 15:29–36.

Spiegelhalter DJ, Best NG, Carlin BP, van der Linde L (2002) Bayesian measures of model complexity and fit. J R Stat Soc Series B Stat Methodol 64:583–639.

Stelmach LB, Herdman CM (1991) Directed attention and perception of temporal order. J Exp Psychol Hum Percept Perform 17:539–550.

Tagliazucchi E, Laufs H (2014) Decoding wakefulness levels from typical fMRI resting-state data reveals reliable drifts between wakefulness and sleep. Neuron 82:695–708.

Twomey DM, Murphy PR, Kelly SP, O'Connell RG (2015) The classic P300 encodes a build-to-threshold decision variable. Eur J Neurosci 42:1636–1643.

Valero-Cabré A, Amengual JL, Stengel C, Pascual-Leone A, Coubard OA (2017) Transcranial magnetic stimulation in basic and clinical neuroscience: a comprehensive review of fundamental principles and novel insights. Neurosci Biobehav Rev 83:381–404.

van Kempen J, Loughnane GM, Newman DP, Kelly SP, Thiele A, O'Connell RG, Bellgrove MA (2019) Behavioural and neural signatures of perceptual decision-making are modulated by pupil-linked arousal. eLife 8:e42541.

Wang CA, Baird T, Huang J, Coutinho JD, Brien DC, Munoz DP (2018) Arousal effects on pupil size, heart rate, and skin conductance in an emotional face task. Front Neurol 9:1029.

White CN, Poldrack RA (2014) Decomposing bias in different types of simple decisions. J Exp Psychol Learn Mem Cogn 40:385–398.

Wiecki TV, Sofer I, Frank MJ (2013) HDDM: hierarchical Bayesian estimation of the drift-diffusion model in Python. Front Neuroinform 7:14.

Yeo BT, Krienen FM, Sepulcre J, Sabuncu MR, Lashkari D, Hollinshead M (2011) The organization of the human cerebral cortex estimated by intrinsic functional connectivity. J Neurophysiol 106:1125–1165.

Yeung AWK, Tzvetkov NT, Atanasov AG (2018) When neuroscience meets pharmacology: a neuropharmacology literature analysis. Front Neurosci 12:852.

Zhang J, Rittman T, Nombela C, Fois A, Coyle-Gilchrist I, Barker RA, Hughes LE, Rowe JB (2016) Different decision deficits impair response inhibition in progressive supranuclear palsy and Parkinson's disease. Brain 139:161–173.